Instantaneous modal identification under varying structural characteristics: A decentralized algorithm

Instantaneous modal identification under varying structural characteristics: a decentralized algorithm

Said Quqa[a,*], Luca Landi[a], Pier Paolo Diotallevi[a]

[a] *Department DICAM, University of Bologna, Viale Risorgimento 2, 40136 Bologna, Italy*

ABSTRACT

One of the latest trends in structural health monitoring involves the use of wireless decentralized sensing systems, developed to reduce costs and speed up the whole monitoring process. The main purpose of this paper is to present a novel decentralized procedure for the instantaneous modal identification of time-varying structures, also suitable in the presence of environmental variations and non-stationary ambient excitation. In particular, a modal assurance criterion (MAC)-based clustered filter bank (CFB) is obtained, capable of decomposing structural responses into modal components for the evaluation of time-varying natural frequencies and modal shapes through a nonlinear energy operator. The proposed algorithm is relatively simple and usable with low-cost smart sensing systems, as it requires low computational effort and works with few data at a time. To prove the effectiveness of the presented method, a simulated near-real-time modal identification procedure has been performed on a full-scale bridge under progressive damage scenarios. The estimated modal parameters have then been used for damage diagnosis. The results reveal a good correspondence between identified modal parameters and reference values, showing also promising outcomes for both damage detection and localization.

KEYWORDS: output-only modal identification; structural health monitoring; wavelet filters; Teager energy operator; damage identification.

Declaration of interests: none.

1. INTRODUCTION

Most engineering structures exhibit characteristics that vary with time. Some variations, for example due to environmental effects (e.g., temperature and humidity) or degradation of structural performance, are slow or infrequent. For the purposes of structural health monitoring (SHM), it is possible to apply the classical methods for identifying modal parameters even in the presence of such variations, assuming the quasi-stationarity of the system [1]. In this way, it is also possible to plan data acquisition intervals, checking the structural state of health periodically [2,3]. For other time-varying systems [4], such as bridges with vehicular traffic [5-7], civil structures in evolving construction phases [8-10], rotating machinery under variable load conditions [11], time-periodic systems like wind turbines [12], robotic or aerospace structures with variable geometry

* Correspondence to: Said Quqa, Department DICAM, University of Bologna, Viale Risorgimento 2, 40136 Bologna, Italy, e-mail: said.quqa2@unibo.it
E-mail addresses: said.quqa2@unibo.it (S. Quqa), l.landi@unibo.it (L. Landi), pierpaolo.diotallevi@unibo.it (P.P. Diotallevi).

[13,14], the application of classical methods for the identification of modal parameters may not be admissible, since the hypotheses of quasi-stationarity could be far from the real situation. In these circumstances, the instantaneous identification of time-varying dynamic features is preferable. Moreover, real-time approaches may be desirable for visualizing identified parameters or to enable prompt decision making [15].

In recent years, many methods have been presented for the identification of time-varying structures. These techniques can be mainly divided into two categories: time-domain methods, which are generally parametric, and time-frequency-domain methods, generally nonparametric or unstructured. As regards the former category, Poulimenos and Fassois [16] presented a survey of methods based upon time-dependent autoregressive moving average (TARMA) representations for modeling non-stationary random vibration and compared them with traditional non-parametric methods. Among the analyzed methods, the functional-series TARMA based technique, presented in [17], has also been employed to achieve damage identification [18]. In further developments, Spiridonakos and Fassois [19] presented a novel class of adaptable functional series TARMA models whose basis functions are estimated based on the modeled signal, while Yang et al. [20] faced the problem of sudden changes proposing a Moving Kriging (MK) shape function modeling method.

As for non-parametric methods, those based on the Hilbert-Huang transform (HHT), the short-time Fourier transform (STFT), and the wavelet transform (WT) are among the most used. Different algorithms based on these techniques have been presented by Nagarajaiah and Basu [21] to demonstrate the ease of implementation and the capabilities of time-frequency methods for modal identification in output-only conditions. The abilities of these techniques to track time-varying modal parameters have been also demonstrated by Kijewski and Kareem [22]. Moreover, different solutions to separate non-stationary multicomponent signals have been proposed. Klepka and Uhl [1] presented an adaptive wavelet-based filtering method, while Wang et al. [23] exploited the limited memory recursive principal component analysis. Both these techniques are based on the assumption of slowly time-varying systems. Bhowmik et al. [4] presented an efficient algorithm to perform blind source separation (BSS) in real time involving a recursive canonical correlation analysis (RCCA), while Amini and Ghaseni [24] used the equivariant adaptive separation via independence (EASI) approach. Ditommaso et al. [25] used a band-variable filter based on the Stockwell transform, employed in further studies [26,27] for damage diagnosis. This method, however, requires prior knowledge of the entire signal in order to perform the analysis.

Some SHM applications may involve limited space for sensor installation, obstacles which may hinder cable deployment, and continuous movement of the workforce which could damage parts of the monitoring system. In these cases, as when the deployment of long cables may increase considerably the overall costs, wireless transmission technologies are preferable [10]. However, continuous high-rate data streaming is impractical through wireless systems, especially for dense sensor networks. Fu et al. [28] proposed an event-triggered sensing system to collect high-fidelity data at the occurrence of strong events, intending to perform prompt decision making with minimal data transmissions. Although this system has shown particularly effective in detecting strong motions, in some applications, damage states may also appear without detectable acceleration peaks, making continuous monitoring preferable.

Recently, technologically innovative wireless sensing systems have been introduced [29-31] that have new generation micro electro-mechanical system (MEMS) sensors connected to microcontrollers capable of performing simple onboard operations. Their limited computational capacity can be exploited through decentralized algorithms [32] in which part of the signal processing procedures (e.g., filtering and downsampling) is performed at the node level. In this way, the data transferred to the monitoring station are lighter and the computational burden is significantly reduced, making it easier to carry out the online monitoring process.

Several authors [33-35] proposed decentralized-topology algorithms based on traditional time-domain or frequency-domain identification methods. These identification techniques are based on the strict assumption of uncorrelated white noise input excitation, not always verified, especially in case of continuous monitoring under environmental conditions. Recently, Yun et al. [36] implemented a new method suitable for wireless smart sensor nodes employing wavelet entropy analysis. In this study, the excitation has been assumed as band-limited white noise. Sadhu and Narasimhan [37] proposed a static filtering method based on the stationary wavelet packet transform (SWPT) for signal decomposition, and Fourier transform for identification of modal parameters. Other authors presented methods based on HHT, that however is not suitable for online applications in the traditional form because of its "global" rather than "local" nature [38]. Wang and Chen [39] proposed a method for online identification of time-varying properties of structures employing a recursive HHT-based procedure. Bao et al. [40] applied the HHT on cross-correlated data windows to improve the robustness to noise contamination. To avoid the difficulties related to the Hilbert transform, as the computation of analytical signals during online applications, some authors experimented with other techniques for the extraction of instantaneous parameters. Ghazali et al. [41] presented a comparative study illustrating the performance of Hilbert transform and other methods, as cepstrum, direct quadrature, and Teager energy operator (TEO), showing how the last is simple and suitable for online applications, but very sensitive to noise. Moreover, this method can only be applied to mono-component signals and therefore requires prior decomposition.

Battery life is one of the most critical issues for wireless monitoring systems, especially when continuous onboard procedures are implemented. Nevertheless, processing and transmissions can be optimized [42], considering an acceptable latency in parameter identification and gaining in network efficiency.

The main contribution of this work is to present a new method for modal identification capable of estimating instantaneous natural frequencies and modal shapes in near real time, even under non-stationary excitation and during changes in structural behavior due to environmental effects or damage. The algorithm consists of two steps. The first involves an initialization procedure in which a wavelet clustered filter bank (CFB) is defined by analyzing a window of acquired signals. By performing the discrete wavelet transform and a clustering procedure based on the modal assurance criterion (MAC) coefficients, it is possible to define the parameters of a filter bank by which modal responses can be directly extracted from the acquired signals by convolution. In a second step, after filter bank construction, microcontrollers at the node levels are able to extract, downsample, and transfer modal responses to the central monitoring station, where the data can be analyzed by means of modal identification techniques as responses of single degree of freedom (SDOF) structures through a TEO-based procedure. Due to the filtering procedure, the noise

sensitivity of TEO is mitigated. Since the modal parameters may vary consistently if damage or strong variations in environmental conditions occur, a recursive updating of the CFB could be necessary. In this context, an adaptive variant to the two-step CFB decomposition algorithm is also proposed.

The main advantages of the presented method are listed below, along with the related assumptions:

- Since the extraction of modal responses is achieved by filtering the data through signal-adapted CFB and the estimation of instantaneous frequencies is performed by means of a local method which considers only few samples, the identified modal parameters are time-dependent. Therefore, the method proposed is capable of tracking the variations of modal parameters due either to varying environmental or operational conditions, or ongoing damage, assuming that the signal window used to generate the filter bank (or most of them in case of the adaptive procedure) is recorded under broadband excitation;
- The method is capable of identifying also abrupt changes in modal parameters in near real time (considering the delay introduced by filtering). For the two-step procedure, the ability to identify changes in modal shapes and natural frequencies is related only with the entity of changes in terms of frequency. For the adaptive variant it depends also on setup parameters (i.e. how frequently the filter bank is updated);
- The continuous signal decomposition is not affected by the end-effects of windowing functions, but only by delay, which depends on the filter bank size;
- The method is relatively simple and suitable for the innovative wireless smart sensor networks (WSSN) since most of the computational burden can be spread throughout the sensing system.

Following a summary of the theoretical background and the description of the proposed algorithm, the second part of this paper is focused on the application of the proposed method to a real case study. In particular, the algorithm has been validated using the data recorded during an experimental campaign performed by the Vienna Consulting Engineers (VCE) together with the University of Tokyo in 2008 on the S101 Bridge, in Austria. The results of instantaneous modal identification are reported and discussed, illustrating a comparison between the identified parameters and the analyses conducted by the VCE. Moreover, as a practical example of exploiting the identified parameters, a simulated near-real-time flexibility-based damage identification procedure is also performed.

2. WAVELET TRANSFORM AND FILTER BANKS

Wavelet transform is a widely used instrument in the field of signal processing, as an alternative to the Fourier transform, especially when dealing with non-stationary signals, since it is capable of capturing both time and frequency information [21-23,43,44].

One of the most used versions of WT is the “non-redundant” discrete wavelet transform (DWT), which entails the application of a recursive filter bank, consisting of low-pass and high-pass filters [45]. For each subsequent transformation level, only the approximations (obtained from low-pass filtering) are further filtered. Although this transform is characterized by a low computational effort, a drawback is that it does not possess the time-invariance property and therefore it is not

suitable for real-time processing of non-stationary signals [46]. Another widely used version of WT is the wavelet packet transform (WPT), in which both the details and the approximations are decomposed at each level. If the WPT coefficients are not decimated after each filter bank application, the transform is known as stationary wavelet packet transform (SWPT). In this version, the analyzed signal is transformed into a series of components characterized by a narrow frequency band, each with the same number of samples of the original signal. Given the redundancy, SWPT is characterized by the shift-invariance property, which makes it ideal for estimating dynamic parameters in real time [47,48].

Wavelet filter banks can be built both to decompose (analysis filters) and reconstruct (synthesis filters) the signal [49]. In order to build such filters, three fundamental parameters have to be determined: the type of function, its order, and the transform level. The first parameter consists of the choice of the function by which the basis of transformation is generated [49]. The second parameter is related to the number of vanishing moments: the higher the number of vanishing moments, the more the filter is close to an ideal one (involving an increase of the support size, i.e., filter length) [50]. The third parameter specifies how many times the transform has to be performed.

The choice of these parameters depends on the purposes of the analysis: in the field of structural health monitoring, several authors use Daubechies [50,51], Symlet [52], and Meyer [53] functions, selecting the wavelets and their orders to be effective with the implemented algorithms. In Fig. 1, six different choices of decomposition parameters are compared as an example (the decomposition level is fixed to 4 for each graph). In particular, the diagrams in the first column show the comparison between the Fejér-Korovkin function of order 14 and the Daubechies function of order 7, which have the same filter length. The gray area represents the filter overlap, corresponding to undesired frequency bands included in the designed bandpass filters. The larger this area, the higher is the eventuality of obtaining multi-component responses as an output of the decomposition procedure (i.e., representing more than one modal response). As reported in [54,55], filter length being equal, the Fejér-Korovkin filter is the closest to an ideal sinc (i.e., cardinal sine) bandpass filter. It can also be noted from Fig. 1 that, even doubling the filter length (see Appendix B for more details on the filter length), Daubechies and Symlet functions (db14 and sym14) are still characterized by higher error when compared to the Fejér-Korovkin function.

Once the decomposition filter bank is built, a convolution of the signal for each generated filter has to be carried out in order to perform the transform. At the last level (n), for the SWPT, 2^n series of coefficients are generated, each referred to a frequency band whose characteristics depend on the chosen parameters. In particular, the higher the transform level, the narrower is the frequency content for each wavelet component. Moreover, the higher the order of wavelet function, the more condensed is the energy in the frequency domain.

It is also possible to reconstruct the original signal from the set of wavelet coefficients by performing the sum of convolutions computed between each wavelet component and the corresponding synthesis filter [49].

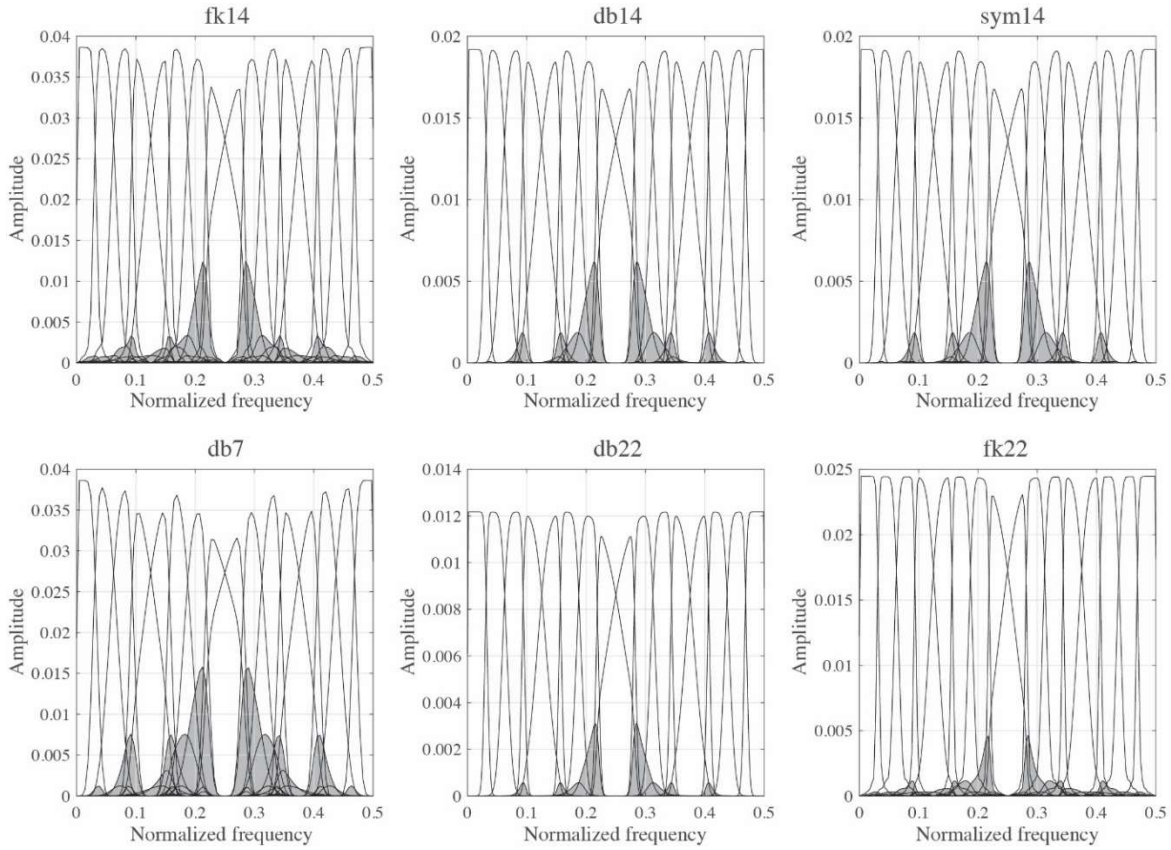

Fig. 1: Comparison of decomposition filter banks in frequency domain (decomposition level 4).

3. DETAILS OF THE ALGORITHM PROPOSED

An identification procedure is suitable for WSSN-based systems if the algorithm is designed in order to allow each node to perform part of the processing operations independently, without knowing the information collected by the other nodes. Moreover, in order to perform the identification procedure in near real time, onboard operations must be simple and fast since the computational capacity of nodes is usually low.

In this context, we propose a two-step identification method (Fig. 2): the first phase (i.e., initialization step) consists of the construction of a CFB, while the second phase entails real-time analysis. In particular, in the latter phase, the signal is first decomposed into modal components at the node level and then transmitted to the monitoring base, which performs the modal identification.

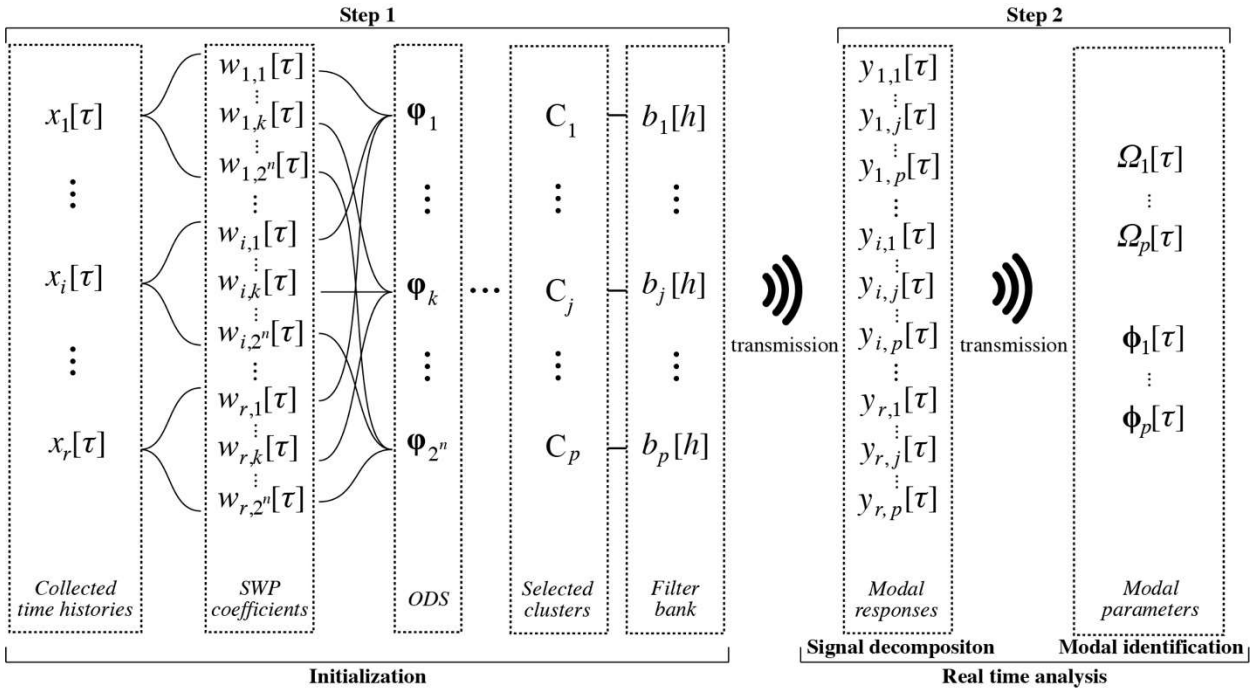

Fig. 2: Workflow of the algorithm presented.

3.1 Choice of the filter bank

In order to implement the n-level wavelet transform of a signal, it can be convoluted with the equivalent filters obtained by cascading the lowpass and highpass filters associated with the selected wavelet, up to level n. The transform is therefore conducted through the application of a filter bank of equivalent filters [49].

In this study, in order to decompose a signal x into a finite set of components y_k characterized by different frequency bands, whose linear combination lead to the original signal, the wavelet decomposition and reconstruction equivalent filters are applied in series, exploiting the perfect reconstruction property of wavelet filter banks [49]. Since the convolution operator $(*)$ is linear and time-invariant [56], a sequence of filtering operations can be performed in any order without changing the output result. It follows that the convolution of the original signal with a decomposition filter and then with a reconstruction filter gives the same output of a convolution between the original signal and the convolution of decomposition and reconstruction filters. By representing the signal and filters as discrete sequences in the time domain:

$$y_k[\tau] = \big((x * d_k) * r_k\big)[\tau] = (x * b_k)[\tau] \tag{1}$$

where y_k is the k-th component of the original signal x, d_k and r_k are respectively the impulse responses of the k-th equivalent decomposition and reconstruction filters corresponding to the selected level of the transform, and b_k is the impulse response of the resulting filter obtained by the convolution between d_k and r_k.

Since convolution is distributive over addition, the filtered version of the signal referred to m frequency bands (from the k_1-th to k_m-th), can be computed as:

$$y_{k_1,k_m}[\tau] = \frac{1}{m}\sum_{k=k_1}^{k_m}(x * b_k)[\tau] = \frac{1}{m}(x * b_{k_1,k_m})[\tau] \tag{2}$$

where b_{k_1,k_m} is a filter obtained by summing the filters b_k associated with the considered m components. By considering the system as linear, time-invariant and causal, the τ-th sample of the filtered signal can be represented as:

$$y_{k_1,k_m}[\tau] = \frac{1}{m}\sum_{h=0}^{N-1} x[\tau - h]\, b_{k_1,k_m}[h] \tag{3}$$

where $N-1$ is the filter order, $N = 2\bar{N} - 1$ is the length of b_k, and $\bar{N}$ is the length of d_k and r_k. From this last relation it emerges that the filtering procedure can be carried out in real time by using only a subset of past samples of the input signal. This process introduces a delay in the output signal, which depends on the choice of parameters used to build the filter bank. Because of the choice of b_k, by properly selecting $k_1, \dots, k_m$, the component y_{k_1,k_m} may be assumed as one of the structural modal responses which are linearly combined in the collected signal x.

3.2 Step 1: Initialization

In a pre-processing stage, each sensor collects an acceleration time history (of user-defined duration) which is directly transmitted to the central monitoring station. Here, the signal collected at each node is decomposed by SWPT, through the convolution with a decomposition filter bank, generating 2^n wavelet components at transformation level n. As discussed in Section 2, each component is related to a different frequency band, the energy of which can be represented by the amplitude of wavelet coefficients.

By selecting a master sensor position (e.g., the first sensor), it is possible to evaluate the operating deflection shapes by computing the mean over time of ratios between the k-th wavelet components of the master time history and other collected signals. In this way, 2^n shapes can be computed as:

$$\varphi_{i,k} = \frac{1}{s}\sum_{\tau=1}^{s}\frac{w_{i,k}[\tau]}{w_{1,k}[\tau]} \tag{4}$$

where $\varphi_{i,k}$ is the i-th element of the k-th operating deflection shape $\boldsymbol{\varphi}_k$, $w_{i,k}[\tau]$ is the τ-th sample of the k-th wavelet component, computed on the signal collected by the i-th sensor, and s is the number of samples for each signal (i.e., the length of the initialization signal window). For more robust results, the average can also be performed after excluding outliers. The MAC coefficient for each couple of shapes (related to the k_1-th and k_2-th components) can then be evaluated as:

$$MAC_{k_1,k_2} = \frac{\left|\sum_{i=1}^{r}\varphi_{i,k_1}\varphi_{i,k_2}\right|^2}{\left(\sum_{i=1}^{r}\varphi_{i,k_1}^2\right)\left(\sum_{i=1}^{r}\varphi_{i,k_2}^2\right)} \tag{5}$$

where r is the number of sensors. In order to generate a filter bank for decomposing the signal through convolution during a following real-time analysis, a clustering procedure is then performed by grouping the consecutive bandpass filters b_k defined in equation (1), the decomposition counterparts of which (d_k) generate wavelet components with similar deflection shapes (i.e., producing high MAC values). In particular, for each couple of consecutive bandpass filters b_{k_1}, b_{k_2}:

$$b_{k_1}, b_{k_2} \in \mathrm{C}_j \iff MAC_{k_1,k_2} \geq t_1 \tag{6}$$

where C_j is a generic cluster, and t_1 is a user-defined threshold. Furthermore, an energy-based selection procedure can be performed to discard the clusters the corresponding global energy E_j of which is lower than a chosen threshold t_2:

$$\mathrm{C}_j \in \Gamma \iff E_j \geq t_2 \tag{7}$$

where Γ is the set of selected high-energy clusters. In this work, the global energy associated with the j-th cluster, which groups the wavelet components from the k_1-th to the k_m-th, has been computed as:

$$E_j = \sum_{i=1}^{r} \sum_{k=k_1}^{k_m} \sqrt{\frac{1}{s} \sum_{\tau=1}^{s} w_{i,k}^2[\tau]} \tag{8}$$

The bandpass filters contained in each selected cluster can thus be summed as shown in relation (2), in order to obtain the resulting filters forming the CFB used in Step 2. The CFB, therefore, consists of bandpass filters by which high-energy signal components associated with different deflection shapes (i.e., decoupled modal responses) are extracted.

The length of the signal window analyzed in the initialization phase is a user-defined parameter that strongly influences the analysis results. In fact, the choice of a short window under non-stationary input excitation could result in a wrong clustering procedure and energy-based selection, since not all the modes of interest could be sufficiently excited. In particular, if the input excitation is characterized by a narrow frequency band, only a low number of vibration modes would be activated, generating low-energy wavelet components associated with the natural frequencies excluded due to the excitation characteristics. In this way, the estimate of operating deflection shapes would be inaccurate due to the low signal-to-noise ratio (SNR) of these components. Moreover, clusters associated with natural vibration modes could also be discarded due to the disturbed energy distribution generated by narrow-band excitation.

At the end of the initialization phase, the monitoring station transmits to each node the CFB, by which the signal decomposition can be directly performed onboard by convolution. It should be noted that, after CFB construction, small variations in frequency and even important variation in modal shapes can be registered since the decomposition is performed by using larger band-pass filters with respect to those associated with single wavelet components, as done in other works [47]. This allows the changes in modal parameters associated with environmental variations or damage to be taken into account in the decoupled modal responses. On the other hand, because

of relations (7) and (8), a signal component must exhibit a persistently high energy value in the interval analyzed during Step 1 in order to imply the inclusion of the corresponding frequency band in the final filter bank. For this reason, high-energy peaks generated by transient features of the non-stationary exciting input are generally filtered out during Step 2, not involving the identification of spurious resonant frequencies. The quality of extracted modal responses could also be further evaluated for example by observing their probabilistic features (e.g., kurtosis [47,57]) in order to discard spurious modes generated by persistent harmonic components in the excitation.

The total complexity of Step 1, as reported in detail in Appendix A, is mainly due to the SWPT and is relatively high compared with that of the rest of the algorithm. However, although low-cost systems could take some seconds to perform the necessary initialization procedures, Step 1 only takes place when particular conditions occur (i.e., at the beginning of the procedure or as described in Section 3.4) and, once finished, gives way to Step 2 that consists of real-time analysis.

3.3 Step 2: Real-time analysis

Once the initialization phase is completed, each node has the same CFB which allows for the real-time decomposition of collected signals into decoupled modal responses, performable independently from other nodes. Therefore, in each node, the signal recorded through the connected sensor is processed by convolution, as shown in equation (3), with each bandpass filter of the CFB generated in Step 1. In particular, to calculate a new sample of the filtered signal $y[\tau]$, a window of new-coming data from $x[\tau - N + 1]$ to $x[\tau]$ with the same length as the filter must be considered. After filtering, each component could also be downsampled (up to the Nyquist rate), in order to reduce the weight of data and easily transmit it to the monitoring station.

After obtaining the decoupled modal responses, these can be analyzed as responses of SDOF structures. In order to implement procedures in real time, a nonlinear energy operator-based local method has been used in this work. In particular, the discrete-time energy separation algorithm-1 (DESA-1), which involves the Teager energy operator (TEO), has been chosen. In the case of discrete signal analysis, the TEO is defined as [58]:

$$\Psi\big[y[\tau]\big] = y^2[\tau] - y[\tau - 1]\, y[\tau + 1] \tag{9}$$

where $y[\tau]$ is the τ-th sample of a digital signal. Several methods have been implemented for the extraction of frequency and amplitude characteristics of non-stationary signals by using this operator [59]. In particular, in DESA-1 [60], the instantaneous digital frequency Ω can be estimated as:

$$\Omega[\tau] \approx \arccos\left(1 - \frac{\Psi\big[z[\tau]\big] + \Psi\big[z[\tau + 1]\big]}{4\Psi\big[y[\tau]\big]}\right) \tag{10}$$

where Ω is the digital frequency, $\omega = \Omega F_s$ is the circular natural frequency, F_s is the sampling frequency, and $z[\tau] = y[\tau] - y[\tau - 1]$. Since in this application the frequency is estimated online (i.e., as new data is available), at the instant τ, the values of $y[\sigma]$ with $\sigma > \tau$ are unknown. For this reason, in equations (9-10), $y[\tau + 2]$ must be intended as the last available value obtained from convolution. In other words, an additional delay of 2 samples is introduced by using this

algorithm for the estimation of instantaneous frequencies. The mathematical description of the total delay is reported in Appendix B.

From each modal response, it is possible to extract an instantaneous trend of the corresponding natural frequency through relation (10). Since a single frequency line per mode is sufficient to characterize the structure over time, it is possible to consider the modal responses extracted at only one sensor position or, alternatively, to evaluate the multivariate instantaneous frequency as an amplitude-based weighted average of the instantaneous frequencies obtained in each position [61], in order to avoid inaccurate estimates due to noisy recordings collected at the nodes of modal shapes. It is possible indeed to capture also the instantaneous amplitude through the TEO [60]. Moreover, as the algorithm uses only a few input samples, it is highly sensitive to noise. In order to remove spikes from the output data, a median filter can be applied on a window of the last $\mu + 1$ estimated values, obtaining the de-noised frequency $\bar{\Omega}[\tau]$ as:

$$\bar{\Omega}[\tau] = median\big[\Omega[\tau-\mu], \Omega[\tau-\mu+1], \Omega[\tau-\mu+2], \dots, \Omega[\tau]\big] \tag{11}$$

An estimation of the i-th element of the j-th instantaneous modal shape $\boldsymbol{\phi}_j[\tau]$ can be simply computed as the ratio between the components $y_{i,j}[\tau]$ and $y_{1,j}[\tau]$ obtained by the convolution of signals registered at different positions (i.e., $x_i[\tau]$ and $x_1[\tau]$) with the same filter b_j:

$$\phi_{i,j}[\tau] = \frac{y_{i,j}[\tau]}{y_{1,j}[\tau]} \tag{12}$$

In this study, the instantaneous estimation of damping has not been considered, for which, to date, robust identification methods are still lacking [62]. Furthermore, damping is not yet clearly correlated with damage and environmental conditions, therefore further studies that go beyond the purposes of this work need to be conducted.

As demonstrated in Appendix A, Step 2 implies a computational burden in the order of $O(N)$ per input sample onboard each node. This makes it possible to obtain near-real-time estimates of instantaneous modal parameters even using low-cost systems (see Section 4.2 for a numeric estimate of timing for the onboard procedures). Most of the traditional identification techniques used in a decentralized fashion for the identification of instantaneous modal parameters require a higher computational burden and are often related to other disadvantages. In particular, processing a signal window of length N through the STFT would imply a computational complexity in the order of $O(N \log N)$ per sample, using the Fast Fourier Transform (FFT) [49]. Moreover, it would also be necessary to extract the instantaneous trend of natural frequencies and modal shapes for each identified mode through a further ridge-extraction procedure, increasing the overall complexity. Considering the HHT, such as in the algorithm used by [40], which does not require ridge extraction, the computational burden can be considered as proportional to that of the FFT [63], but the results obtained are often affected by problems such as mode-mixing. Furthermore, in a decentralized topology, the intrinsic mode functions (IMFs) computed by analyzing the signals collected in different positions may have different frequencies (and then be associated with different vibration modes) on each node, leading to a wrong estimation of modal shapes.

The computational cost of Step 2 for the monitoring station is moreover particularly low if compared to other recent centralized algorithms. Considering, for example, the method based on recursive correlation analysis (RCCA) presented in [4], the most demanding part related to the eigenspace update has a complexity in the order of $O(m^3)$ per input sample, with m denoting the number of eigenvectors of the block covariance matrix of structural responses, which depends on the number of data channels and is generally higher than the number of identified modes p which governs the computational complexity of the presented algorithm without considering any post-processing operation (see Appendix A.2). Similarly, the equivariant adaptive separation via independence (EASI) algorithm used in [24] has a complexity in the order of $O(q^3)$ where q is the number of data channels [64]. Moreover, it should be noted that the decentralized fashion of the proposed algorithm enables suitable downsampling of data before transmission, which makes it suitable for wireless systems. On the other hand, the algorithms presented in [4] and [24] require the data from all sensors available in the monitoring station in order to update the time-varying models.

3.4 Adaptive variant of the procedure

During long-term monitoring, modal parameters may undergo higher variations than those allowed by the CFB generated in the initialization phase. In order to improve signal decomposition, the filter bank should thus be periodically updated. The updating procedure consists of a repetition of Step 1 at determined time intervals, at the occurrence of situations in which it may be convenient to update the filter bank (e.g., when the signal amplitude is high, SNR increases and the effects of noise less affect the procedure), or when significant changes are noticed in the evaluated instantaneous frequencies. The updating procedure also reduces the risk of carrying out an incorrect identification based on a filter bank generated in the presence of narrow-band excitation.

If one of the conditions selected to start the updating procedure arises, the sensing nodes collect and transmit a limited signal window to the monitoring station, as it occurs during the initialization phase. Then, the procedures illustrated in Section 3.2 are repeated and the updated CBF is finally transmitted to each node, where real-time analyses start again using the new filters until the next update. The recursive clustering procedure to determine the updated filter bank can be performed by taking into account not only the parameters evaluated within the new signal window but also those computed at previous steps, by performing a weighted average. In particular, we propose the updating procedure described in Fig. 3, in which an average between the new and old MAC coefficients is performed at each updating step, and then used for the clustering procedure.

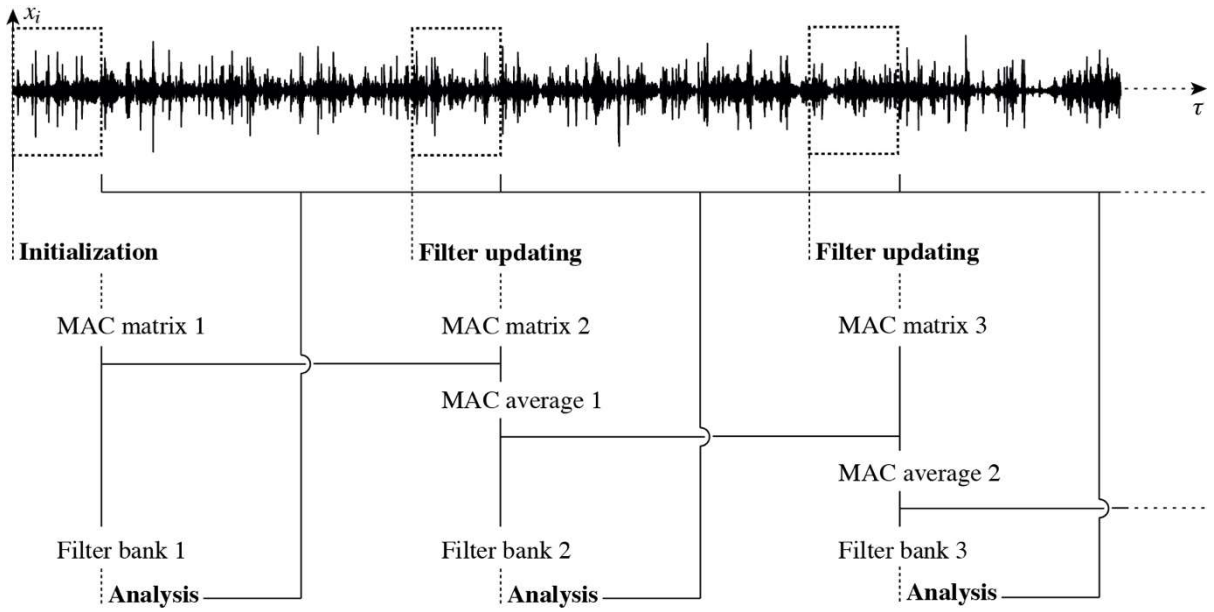

Fig. 3: Workflow of the adaptive method.

The weighted MAC value between the components k_1 and k_2 used during the l-th update is given by:

$$\overline{MAC}^{l}_{k_1,k_2} = \frac{MAC^{0}_{k_1,k_2}}{2^l} + \sum_{\zeta=1}^{l} \frac{MAC^{\zeta}_{k_1,k_2}}{2^{l-\zeta+1}} \tag{13}$$

where $MAC^{0}_{k_1,k_2}$ is the value computed during the first initialization procedure and $MAC^{\zeta}_{k_1,k_2}$ are the values calculated during the subsequent updates, up to the l-th. At each iteration, the new part gains the same weight of the whole set of previous values, the older of which become negligible after a few updates.

If low-cost hardware with limited computational capacity is implemented to realize the monitoring system, it may be necessary to interrupt the real-time analysis during the filter updates, since clustering is an energy-consuming centralized operation (as shown in Appendix A). To limit this issue and optimize resources, the filter update procedure should be shortened as much as possible. For this purpose, a limited number of sensor positions can be selected as a reference and used to calculate the parameters on which the cluster procedure is based. The MAC coefficients can therefore be evaluated considering only the signals coming from the selected reference positions. In this case, relation (5) becomes:

$$\widehat{MAC}_{k_1,k_2} = \frac{\left|\sum_{i=1}^{\hat{r}} \varphi_{i,k_1}\varphi_{i,k_2}\right|^2}{\left(\sum_{i=1}^{\hat{r}} \varphi_{i,k_1}^2\right)\left(\sum_{i=1}^{\hat{r}} \varphi_{i,k_2}^2\right)} \tag{14}$$

where $\widehat{MAC}_{k_1,k_2}$ is the coefficient computed by considering only $\hat{r}$ reference positions, with $2 < \hat{r} < r$. Moreover, if only two reference positions are selected, the average ratio between the

filtered components reported in equation (4) can be directly used as clustering variable. In this case, the condition (6) becomes:

$$b_{k_1}, b_{k_2} \in \mathrm{C}_j \iff \frac{1}{s}\sum_{\tau=1}^{s}\left(\frac{w_{\hat{r}_1,k_1}[\tau]}{w_{\hat{r}_2,k_1}[\tau]} - \frac{w_{\hat{r}_1,k_2}[\tau]}{w_{\hat{r}_2,k_2}[\tau]}\right) \leq t_3 \tag{15}$$

with $\hat{r}_1$ and $\hat{r}_2$ the selected reference positions, and t_3 a user-defined threshold. Using a small number of signals for clustering leads to a consistent reduction in the computational burden of the updating procedure. This can be seen in detail in Appendix A, since the value of r reported in Tab. A.1 decreases to $\hat{r}$. However, this simplified method could lead to the construction of a less accurate filter bank, depending on the choice of master positions. In order to make the optimal selection, the positions have to be chosen at the points where maximum amplitudes of first modal shapes occur, avoiding the nodes, where the recorded accelerations are low and inaccurate.

Both for the original approach and for the simplified method, the computational complexity of the identification procedure, as well as the accuracy and delay of identified quantities, depend on the choice of setup parameters, as shown in Appendices A and B. In particular, the parameters concerning the wavelet transform (i.e., the type of function, its order, and the transform level), the length of post-processing window, the MAC threshold used for filter bank construction, and its updating rate play a central role. The criterion for choosing these parameters may however vary according to the specific case study. For structures with quite distant vibration modes (in terms of natural frequency) and low-noise recordings, it is advisable to build a small filter bank in order to obtain modal parameters with little delay; on the other hand, in the case of noisy recordings and closely-spaced vibration modes, filter order and transform level must be increased, also increasing the delay. In this case, a more frequent filter update may also be necessary. Thus, high transformation levels and wavelet orders lead to more precise filtering, with the disadvantage of higher computational effort and long delays due to demanding convolution procedures. Regarding the MAC threshold, the selection of a low value generally leads to filters with a wider band, which may result in the extraction of modal responses with low SNR or multi-component signals (in the case of consecutive modes with similar shapes). On the other hand, if the decomposition level is high and the signal analyzed is noisy or the window selected for the initialization phase is short, a low threshold could help in merging components of the same vibration mode, the shapes of which are slightly different due to estimation errors. A large value of the threshold however leads to narrow-band filters which must be frequently updated if estimated modal parameters fluctuate either for physical reasons or estimation uncertainties. A practical example of the effects of MAC threshold selection is given in Section 4.2.

It should also be noted that the method presented is designed for the online identification of modal parameters, but it could also be used for periodic inspections. In this case, after the initialization, the sensing nodes could be periodically switched on for collecting signal in a given time interval, which is decomposed and downsampled onboard each node, and then transmitted to the monitoring station. This procedure however allows the reduction of data transmissions, and therefore of energy consumption, since modal responses can be suitably downsampled after filtering. Moreover, time information is preserved, allowing the analysis of short-time non-

stationary sequences recorded for example at the occurrence of strong seismic events or particular operating conditions.

In the case of damage diagnosis for civil structures, it is also important to consider the long-term variability of identified parameters [65,66]. First, the knowledge of their variation under different environmental conditions allows the construction of a statistical distribution that may be used to limit the possibility of false alarms [67,68]. This may be done, for example, by correlating the variation of estimated parameters with measured environmental conditions (such as temperature and humidity) and anthropic sources (such as the intensity of vehicular traffic) [69-71]. Moreover, in order to restrain the fluctuation of identified parameters due to continuously changing operational conditions (e.g., moving cars on a bridge), a suitable post-processing phase is necessary. For example, by using a wide window for median filtering, as shown in equation (11) and Appendix B, the robustness of the algorithm to operational uncertainties will increase, as the latency of resulting identified quantities.

4. APPLICATIONS

In this section, a practical application of the CFB decomposition is shown. The case study analyzed is the full-scale S101 Bridge in Vienna, on which the Vienna Consulting Engineers (VCE), together with the University of Tokyo, conducted an experimental campaign in 2008, collecting acceleration time histories under ambient vibration and different structural health conditions [72-73].

In this work, the data has been analyzed a posteriori, with the complete data set available. However, the analyses are conducted by considering only few samples at a time, simulating a real-time monitoring process.

4.1 Description of the case study configuration

The case study analyzed (Fig. 4 and 5) is a three-span post-tensioned concrete bridge built in the 1960s and demolished in 2008 due to the need for an additional lane underneath. The bridge slab was continuous, supported by two pairs of piers. The central and side spans were respectively 32 meters and 12 meters long. The cross section was 7.2 meters wide, formed by beams with variable height along the longitudinal direction, equal to 0.9 meters in the middle of the central span, up to 1.7 meters at the piers.

Fig. 4: View of the S101 Bridge [72].

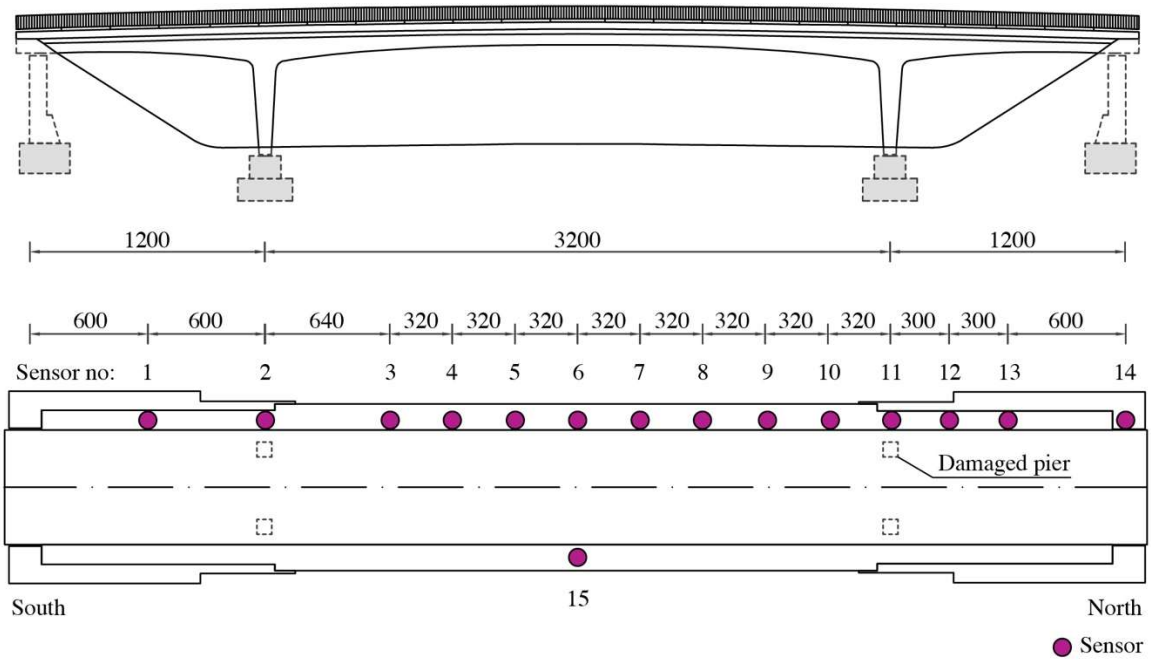

Fig. 5: Configuration of the case study and sensor disposition [72]; dimensions are indicated in centimeters.

Before the demolition, a three-day experimental campaign was carried out, aimed at identifying the structural damage under progressive artificially induced damage scenarios, consisting of north-western pier settlements and loss of post-tension forces. In this application, only the conditions referred to the pier settlement have been considered (summarized in Fig. 6 and Tab. 1). In particular, after unloading the pier by means of a hydraulic jack, it was cut at the base (scenario A) and a slice 10 cm thick was extracted (Fig. 7). Then, the jack was lowered in three progressive steps, each by 1 cm (scenarios B, C, and D). In the first two steps, the pier followed the whole lowering, while at the end of the third step the final measured settlement was 2.7 cm and the column was completely suspended. Afterward, some compensating plates were inserted at the bottom of the pier (scenario E).

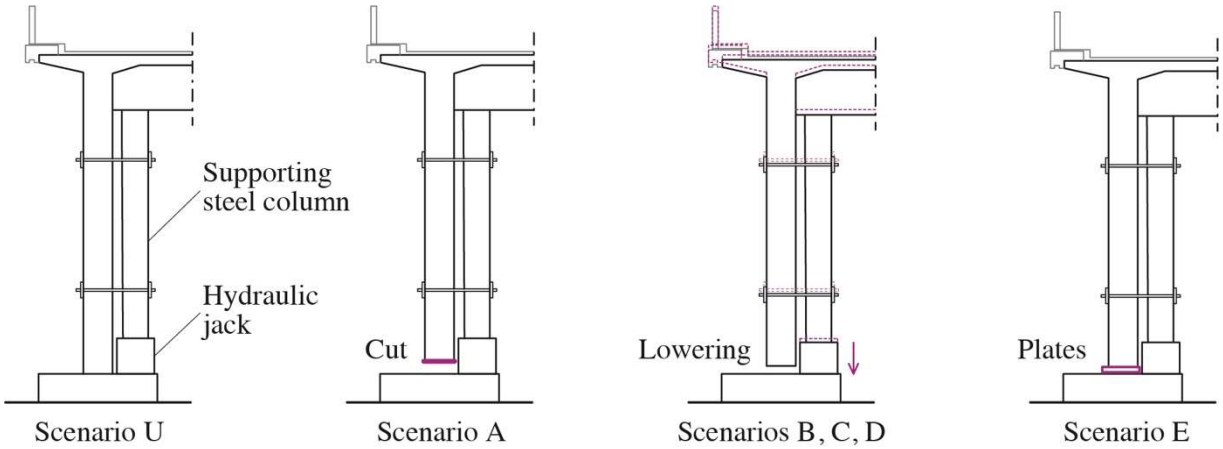

Fig. 6: Schematic of progressively induced damage scenarios.

Tab. 1: Summary of progressively induced damage scenarios

Damage scenario	Description
U	Undamaged structure
A	Cut of the north-western column
B	First step of lowering – 1 cm
C	Second step of lowering – 2 cm
D	Third step of lowering – 3 cm
E	Insertion of compensating plates

Fig. 7: Photographic documentation of the pier settlement process [72].

The data were collected by using a dense BRIMOS [74] sensor grid consisting of 15 three-directional FBA-23 force balance accelerometers from Kinemetrics, with a sensitivity of 2.5 V/g under full-scale range of 1 g, and a resolution of 10^{-6} g. Raw signals were logged by means of a 16-bit analog-to-digital converter (ADC). The sensors were arranged on the structure as shown in Fig. 5: 14 of them were positioned along the west side and 1 along the east side in order to also identify torsional modes. The original data were collected with a sampling frequency of 500 Hz. More details about the geometry and the instrumentation used can be found in [72,75]. In Tab. 2 the results of identification procedures shown in [72] for the scenarios from U to E are reported. The percentage variation of natural frequencies with respect to the undamaged condition have also been computed and noted in Tab. 3. The reference frequencies shown in Tab. 2 were calculated by the VCE using the BRIMOS software, which extracts the peaks of an averaged normalized power spectral density (ANPSD) obtained from windowed data [75].

Tab. 2: Natural frequencies identified during the experimental campaign conducted in 2008, reported in [72]

Mode	Damage scenario					
	U	A	B	C	D	E
1	4.05 Hz	3.95 Hz	3.96 Hz	3.92 Hz	3.62 Hz	3.98 Hz
2	6.30 Hz	6.08 Hz	6.01 Hz	5.88 Hz	5.39 Hz	5.91 Hz
3	9.69 Hz	9.44 Hz	9.44 Hz	9.28 Hz	8.22 Hz	9.34 Hz
4	13.29 Hz	12.15 Hz	11.65 Hz	10.79 Hz	10.06 Hz	10.92 Hz

Tab. 3: Percentage variation of natural frequencies with respect to the undamaged condition (with reference to data reported in Tab. 2)

Mode	Damage scenario				
	A	B	C	D	E
1	-2.47%	-2.22%	-3.21%	-10.62%	-1.73%
2	-3.49%	-4.60%	-6.67%	-14.44%	-6.19%
3	-2.58%	-2.58%	-4.23%	-15.17%	-3.61%
4	-8.58%	-12.34%	-18.81%	-24.30%	-17.83%

4.2 Two-step algorithm implementation

In this paper, only the data recorded in the vertical direction has been used, downsampled at 100 Hz. In order to set up the two-step procedure, a 100-second signal window for damage scenario U, recorded at each sensor position, has been used in the initialization phase. Those signals have been decomposed through a decomposition filter bank built by choosing the 14-th order Fejér-Korovkin wavelet (fk14) and decomposition level 6.

Afterward, the operating deflection shapes associated with each component and their MAC coefficients have been computed as shown in Section 3.2. Then, a clustering procedure has been performed in order to group the components characterized by high MAC value and similar frequency contents. To this aim, a threshold of 0.8 has been chosen for MAC-based clustering, and only consecutive components have been assigned to the same cluster.

Consequently, an energy-based selection procedure has been performed on the obtained clusters in order to select only the high-energy components. In Fig. 8, the bandpass filters associated with the MAC-based clusters are represented in the frequency domain, together with their RMS energy values (represented as circles). In this phase, being interested in the identification of the first modes, only the frequency band from 0 to 15 Hz has been analyzed. Only the clusters with high energy values (i.e., the outliers with respect to the mean) have been selected to form the final CFB, which is then transmitted to the sensor nodes.

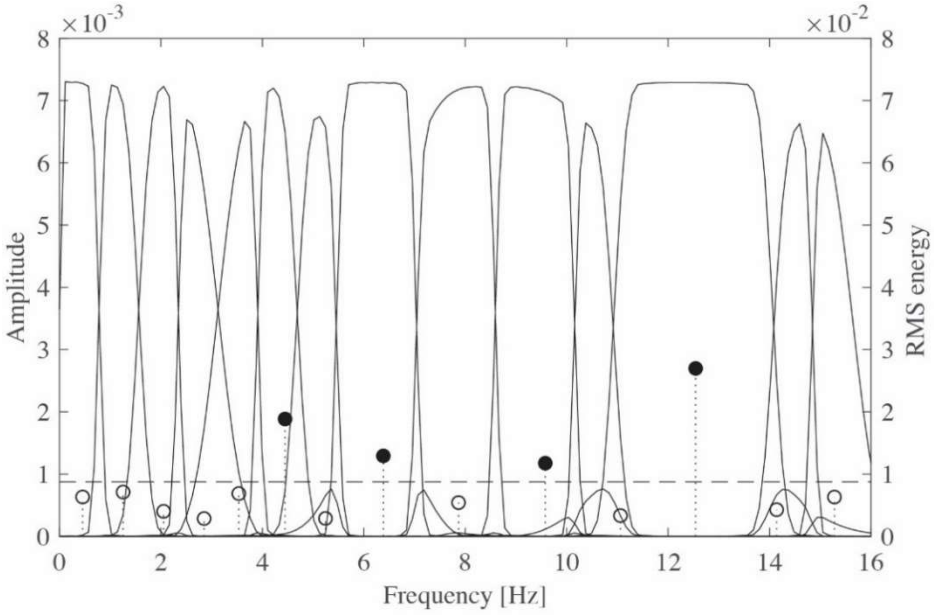

Fig. 8: Representation of the filter bank in the frequency domain and the energy level (RMS) for each cluster (full circles indicate energy values over the average level, represented as a dashed line).

In Fig. 9, the filter banks obtained by selecting different values of MAC threshold are reported. As explained in Section 3.4, higher values lead to narrow-band filters, which may be unsuitable for noisy data. Moreover, the RMS energy threshold for selecting high-energy components changes, generally resulting in a larger number of high-energy components for low values of MAC threshold. Superimposed to the filter banks, in Fig. 9, a tree structure shows how filters are divided as the MAC threshold increases.

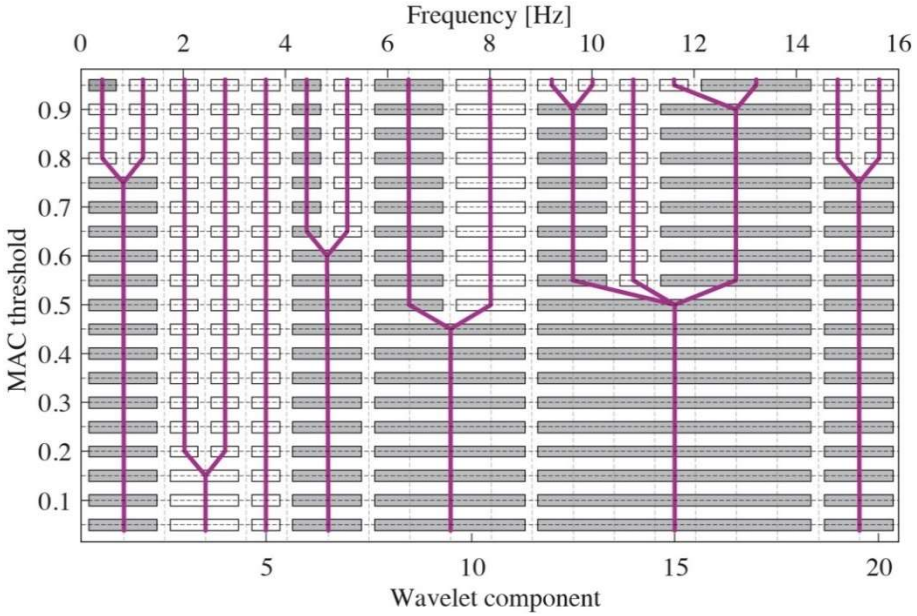

Fig. 9: Filter banks obtained using different values of MAC threshold. Each filter is represented as a rectangle (empty for low-energy components and filled for high-energy components).

Once completed the initialization phase, each node has the filter bank that allows for real-time decomposition. A signal set obtained by merging 6 subsets related to different damage scenarios has been analyzed in order to perform the modal identification under structural time-variant behavior. In particular, 15 acceleration time histories (i.e., one for each sensor position) of 33 minutes have been generated by merging the 5.5 minutes recordings related to scenarios U, A, B, C, D, and E, with reference to Tab. 1. Each signal has been decomposed individually, simulating the operations performed onboard every sensor node (i.e., convolution with the CFB).

While the decomposition is in progress, each sample obtained by convolution (or a subset of them in case of downsampling) can be transmitted to the monitoring station, which performs the real-time modal identification. In this application all the modal responses have been downsampled by a factor 3 (with a final sampling period of 0.03 seconds). Natural frequencies and modal shapes have been estimated through the use of TEO, as shown in Section 3.3. In order to obtain more accurate results, a median filter has been applied using a window of 300 samples (i.e., each sample of the resulting instantaneous parameters has been computed as the median of the last 300 instantaneous values). The results in terms of frequency, which in this study have been computed

only considering the signal collected by sensor 9, are reported in Fig. 10, where the trend obtained in this analysis is also compared with the reference values of Tab. 2, with the natural frequencies obtained by performing a frequency domain decomposition (FDD) over each damage scenario, and with the trend computed by using the adaptive technique, as shown in Section. 3.4, which will be discussed in the next section. In the figure, these plots are also superimposed on the spectrogram obtained by means of the STFT performed on the unfiltered signal collected in the same position.

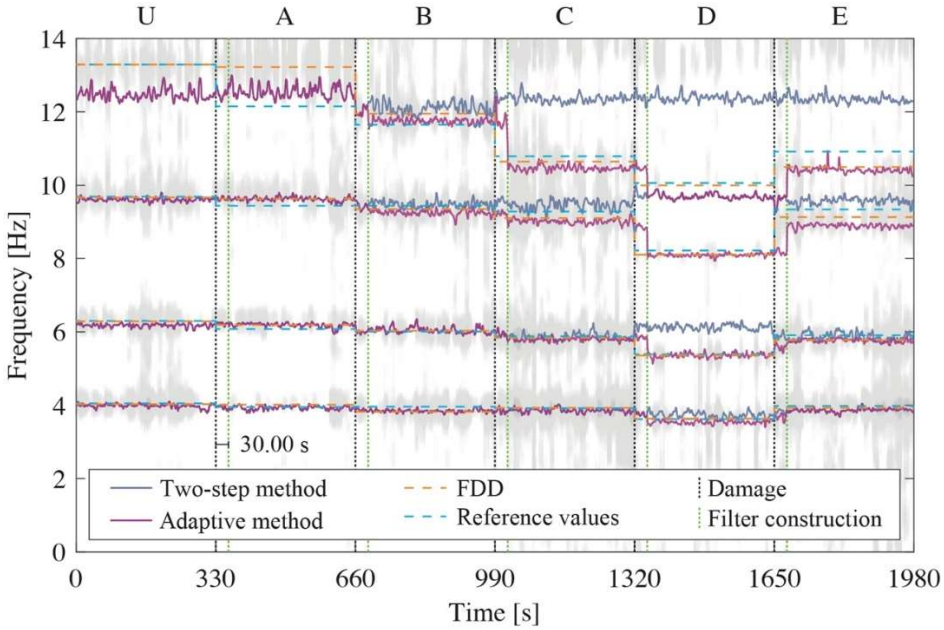

Fig. 10: Comparison of identified natural frequencies over time. The lines of identified frequencies are superimposed on the spectrogram obtained by means of STFT (gray shade).

In Fig. 10, the vertical black dashed lines represent the entry into a different damage condition. In this figure, the identification latency due to convolution, DESA-1 algorithm, and median filtering is not represented. It can be computed as shown in Appendix B, resulting respectively in 8.76, 0.06 and 4.50 seconds (i.e., 876 samples under the original sampling frequency, and 152 samples after downsampling by a factor 3), for a total of 13.32 seconds. This latency would involve a uniform translation of the diagrams in Fig. 10 to the right.

In Tab. 4, the average frequency values identified for each damage condition are reported, along with the percentage difference between identified and reference values of Tab. 2. It is possible to notice how, for small variations in the natural frequencies, the results of the two-step procedure are in agreement with reference values and coincide with those of the adaptive variant, since the filters in CFB have the same cut-off frequencies. On the other hand, when considerable variations occur, a static CFB leads to increasing errors in identified modal parameters, especially for higher modes. In these cases, an adaptive updating in preferable.

Tab. 4: Average natural frequencies identified through the proposed algorithm and percentage difference with respect to reference values of Tab. 2

Mode	Algorithm	Damage scenario					
		U	A	B	C	D	E
1	Two-step	3.98 Hz [-1.73%]	3.93 Hz [-0.51%]	3.85 Hz [-2.78%]	3.85 Hz [-1.79%]	3.73 Hz [+3.04%]	3.86 Hz [-3.02%]
	Adaptive	3.98 Hz [-1.73%]	3.93 Hz [-0.51%]	3.85 Hz [-2.78%]	3.85 Hz [-1.79%]	3.56 Hz [-1.66%]	3.85 Hz [-3.27%]
2	Two-step	6.18 Hz [-1.90%]	6.19 Hz [+1.81%]	6.04 Hz [+0.50%]	5.87 Hz [-0.17%]	6.13 Hz [+13.73%]	5.87 Hz [-0.68%]
	Adaptive	6.18 Hz [-1.90%]	6.19 Hz [+1.81%]	6.04 Hz [+0.50%]	5.80 Hz [-1.36%]	5.41 Hz [+0.37%]	5.74 Hz [-2.88%]
3	Two-step	9.61 Hz [-0.83%]	9.62 Hz [+1.91%]	9.47 Hz [+0.32%]	9.46 Hz [+1.94%]	9.70 Hz [+18.00%]	9.57 Hz [+2.46%]
	Adaptive	9.61 Hz [-0.83%]	9.62 Hz [+1.91%]	9.27 Hz [-1.80%]	9.03 Hz [-2.69%]	8.16 Hz [-0.73%]	8.83 Hz [-5.46%]
4	Two-step	12.47 Hz [-6.17%]	12.55 Hz [+3.29%]	12.10 Hz [+3.86%]	12.36 Hz [+14.55%]	12.38 Hz [+23.06%]	12.34 Hz [+13.00%]
	Adaptive	12.47 Hz [-6.17%]	12.55 Hz [+3.29%]	11.77 Hz [+1.03%]	10.58 Hz [-1.95%]	9.76 Hz [-2.98%]	10.34 Hz [-5.31%]

In Fig. 11, the identified modal shapes are represented over time: the plotted mesh interpolates the values estimated by sensors 1-14, while the black line plotted on the time-amplitude plane represents the component associated with sensor 15, positioned on the opposite side of the bridge.

In Fig. 12, the MAC coefficients computed by using the modal shapes identified through the two-step method and those reported in [72] are shown. In particular, each MAC coefficient has been computed considering the modal shape identified by means of the algorithm proposed, averaged over the entire duration of the considered damage scenario, and the corresponding modal shape (i.e., related to the same mode and damage scenario) reported in [72].

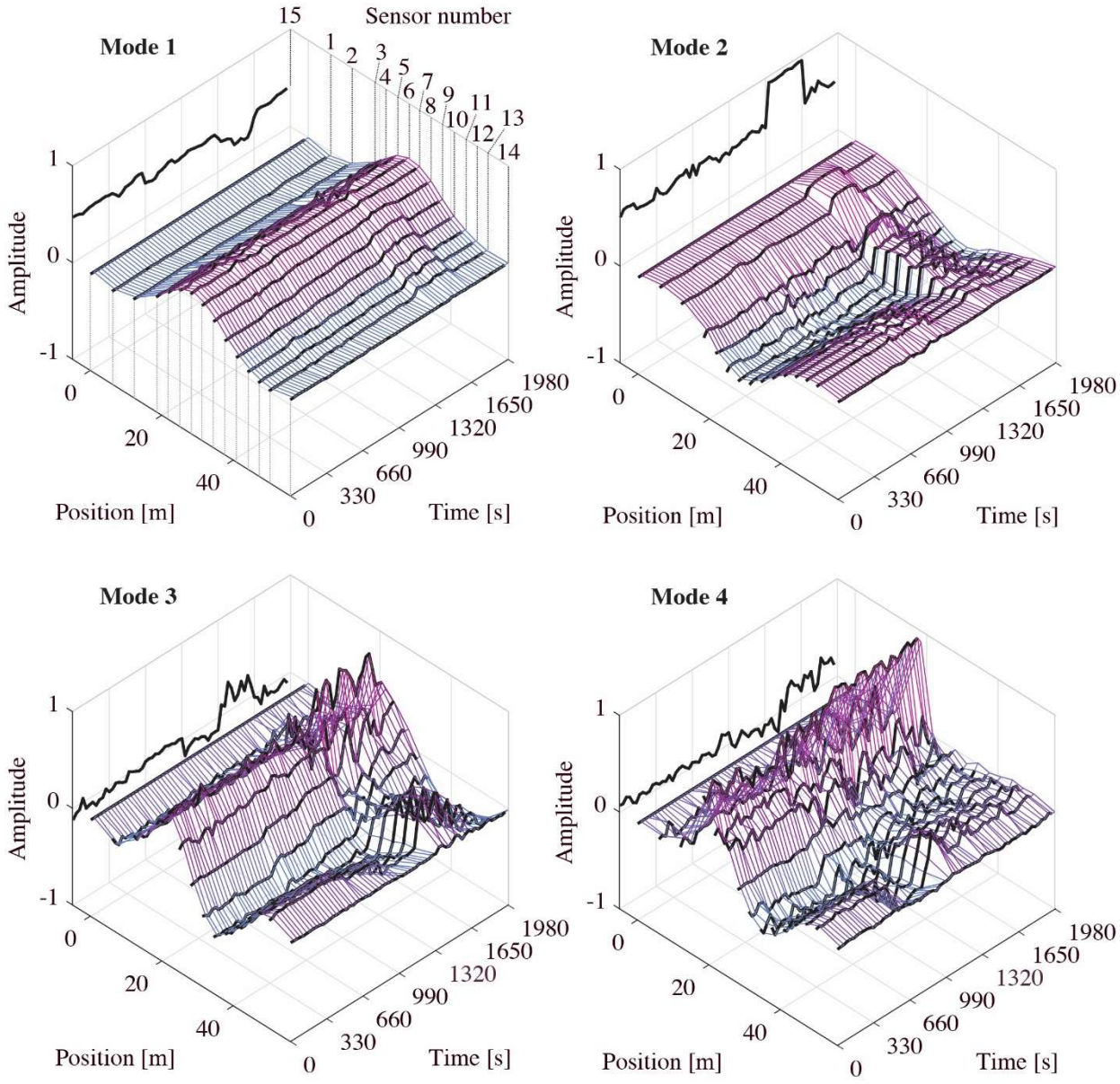

Fig. 11: Mesh interpolation of the instantaneous modal shapes identified by the two-step method.

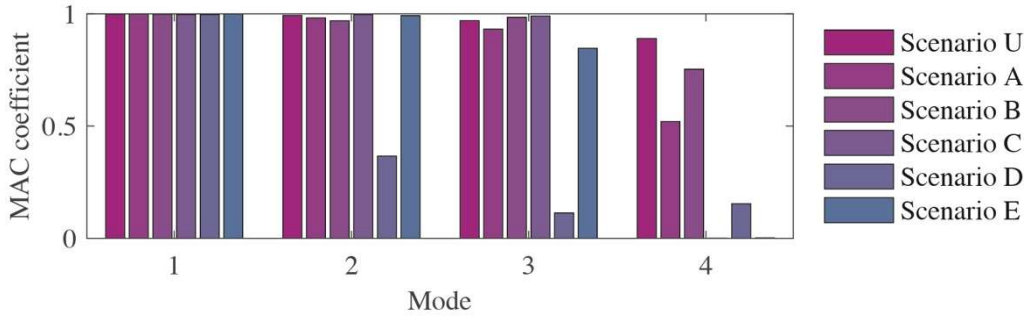

Fig. 12: MAC coefficients computed by using the averaged modal shapes identified through the two-step method and those reported in [72].

From these results, it can be noted that both in terms of frequencies and modal shapes, the first mode has been successfully identified for all the damage scenarios, since the variation in terms of frequencies are modest (see Tab. 3) and the CFB generated in the initialization phase is able to catch the whole frequency band associated with the evolution of the selected mode over time. As concerns the second mode, the two-step CFB decomposition e is efficient for all the damage scenarios except for condition D, in which the percentage variation in terms of frequency is about 15%. The fourth mode is characterized by frequency variations higher than 10% already for condition B, and therefore the identification results are poorly accurate for the following scenarios.

While for the monitoring station Step 2 is much less demanding than Step 1 in terms of computational complexity, considering also that the monitoring station generally consists of a wired system with a larger computing footprint, the computational cost of Step 2 is of fundamental importance for sensing nodes. As shown in Appendix A.2, the computational complexity of step 2 for sensing nodes depends on the number of filters (i.e., the number of modes identified) and their length. In this application, considering 4 modes extracted by using filters of 1753 taps each (see Appendix B for more details), a total amount of 7012 multiply-accumulate operations is performed for decomposing each new sample of data by convolution. In particular, the signed long multiply with accumulate (SMLAL) instruction is considered, which is more suitable for high-accuracy signal processing (e.g., when operating with 16-bit or 24-bit ADC data) [76]. Considering, for example, the low-power X-scale PXA271processor (i.e., the same implemented on the Imote2, an advanced platform largely used for SHM purposes [2,31,32]), working at 13 MHz, and assuming an average value of 4 cycles per instruction (CPI) for the SMLAL [77,78], each new sample of data requires an execution time of about 2.15 ms to be decomposed into four separate double-precision samples of modal responses. The reason why an average value is selected for the number of cycles is that it depends on the early termination of registers. However, the selected value is precautionary, as it is exceeded only in the event of an overflow [76-78]. It is also possible to optimize the convolution procedure using the integrated performance primitives (IPP) [78], achieving even better performances.

Simulating the extraction of four modal responses from a signal of 2048 samples by means of the method proposed, about $57.442 \cdot 10^6$ clock cycles are overall necessary, regardless of the nature of the signal analyzed. The HHT is one of the most used methods for the identification of instantaneous frequencies and amplitudes in different fields of engineering. In particular, recent implementations in the civil field have been proposed [29], together with online variants [63] which enable the real-time extraction of modal responses [39,40]. Implementing onboard each node the empirical mode decomposition (EMD), that is the first step of the HHT in which the signal is decomposed into IMFs, the computational cost would be strongly related to the signal features [79] and could be different for each node. Wang et al. [79] measured an average of $22.528 \cdot 10^6$ clock cycles per extracted IMF on an electrocardiography (ECG) signal of 2048 samples processed through a Nios II processor and using the stopping criterion proposed in [80]. However, a simulation of the most time-consuming condition, analyzed in the same work, lead to $1.380 \cdot 10^6$ clock cycles per sifting iteration, which is more than 10 times higher than the initial test with the ECG signal. Considering the computational complexity estimated by [63] in the worst case, instead, the total number of cycles involved in the decomposition of a 2048-sample sliding

window with extra 256 samples overlap (in both sides, for a total of 2560 samples) for the extraction of 11 IMFs (assuming EMD as a dyadic filter bank) is $55.757 \cdot 10^6$, which is comparable with the effort of the presented algorithm. In this evaluation, 10 sifting iterations have been assumed per IMF; moreover, 3 clock cycles have been assumed for simple multiplications, 1 for additions, 1 for comparisons, and 50 for divisions, which can generally take between 20 and 100 cycles [77]. However, IMFs have not pre-determined frequency values and it is difficult to discern between physical and noise-generated components onboard the microcontroller, requiring the transmission of all identified IMFs without downsampling. This issue makes online implementations on WSNs unfeasible. Comparing the method proposed with another wavelet-based approach for online identification of modal parameters presented in [1], the computational complexity of the signal decomposition part is exactly the same since it involves a filtering process through an adaptive wavelet filter bank. However, the wavelet function selected in [1] is complex, increasing the necessary number of cycles per operation, and the online recursive least squares algorithm for the identification of modal parameters is not suitable for onboard processing and filter updating since it requires matrix multiplications at each data sample acquired. Moreover, a centralized identification of modal parameters with instantaneous feedback updating of the filter bank would involve high wireless transmission rates, making the algorithm unsuitable for implementation on WSNs.

4.3 Adaptive algorithm implementation

In order to mitigate the problems associated with a static definition of the CFB, an adaptive procedure can be applied by updating the filter bank at user-defined intervals or at the occurrence of particular conditions (e.g., upon reaching a user-defined variance value in the modal parameters estimation). In Section. 3.4 of this paper, an adaptive variant of the decomposition algorithm has been proposed, and the related results are discussed in this section.

To evaluate the efficacy of the proposed method, the identification has been performed by considering the first CFB as the one already used in Section. 4.2, followed by 5 updating steps (one every 5.5 minutes, at the beginning of the signal segments related to different damage conditions). For each step, a signal decomposition has been carried out by considering a time window of 30 seconds, and the matrix of MAC coefficients has been computed by using the operating deflection shapes of each signal component. With the aim of speeding up the procedure, the decomposition can be carried out by considering a reduced frequency band: in this work, only the interval [0-15 Hz] has been considered. The MAC matrices related to each updating step are reported in Fig. 13 (first row). In order to avoid the inaccurate estimation of modal parameters due to the inefficient choice of the signal windows necessary to build the filter banks, an average procedure has been performed on the MAC matrices, as explained in Section 3.4. For each step, the novel filter bank is then evaluated by using the related averaged MAC matrix, reported in the second row of Fig. 13 for each update.

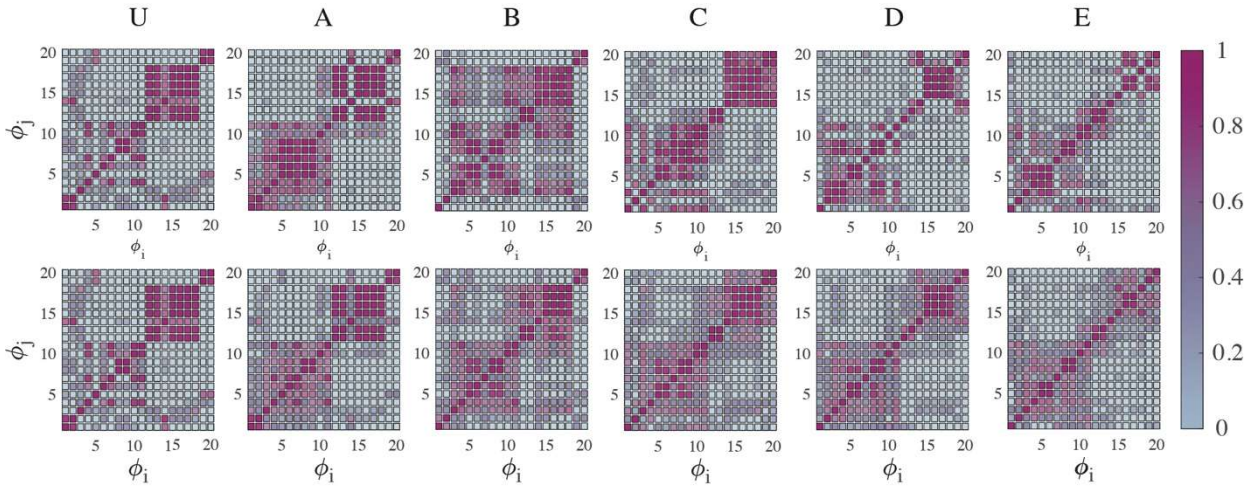

Fig. 13: MAC matrices computed for each step (first row) and related average matrices used for updating the CFB (second row).

It is observable that high values in the MAC matrices related to the condition A are quite widespread (not only close to the diagonal), but the matrices used to build the filter banks are less sensitive to this fact due to the performed average procedure. In Fig. 10, 14 and 15 the instantaneous modal parameters identified through the adaptive method are shown, together with the related MAC coefficients, computed by using the modal shapes reported in [74] as references.

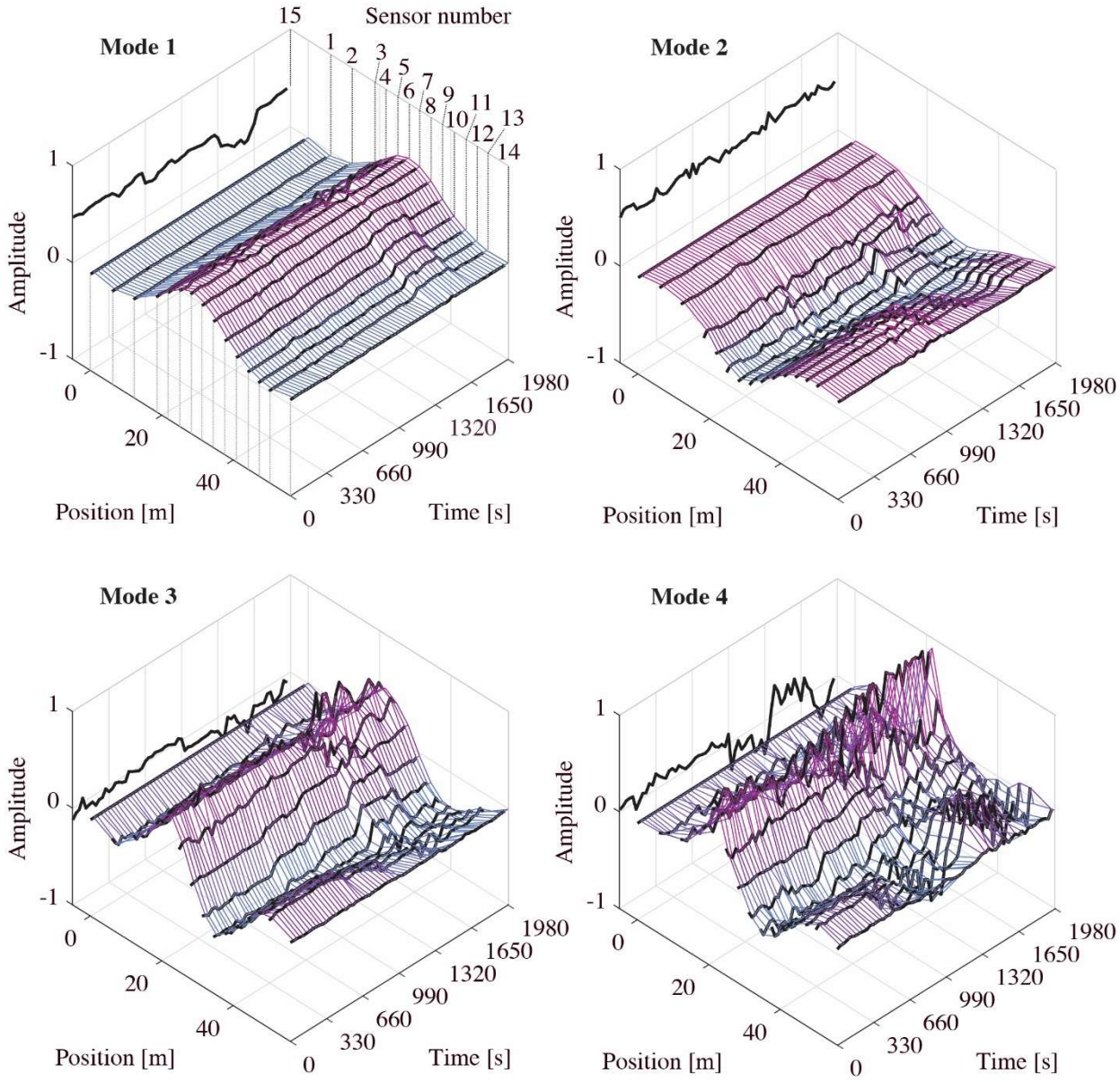

Fig. 14: Mesh interpolation of the instantaneous modal shapes identified by the adaptive method.

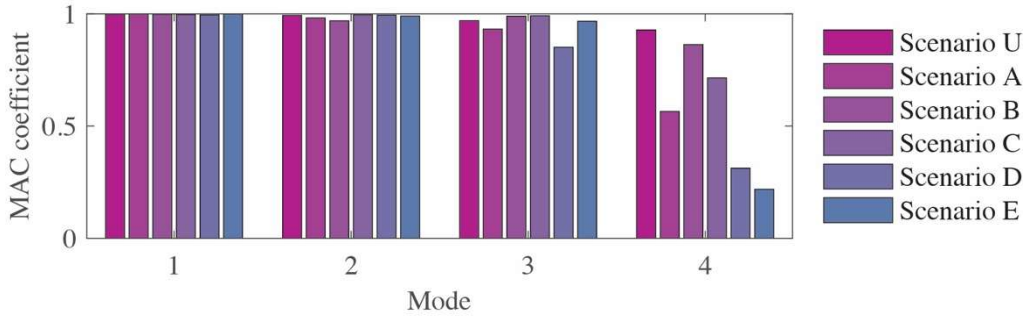

Fig. 15: MAC coefficients computed by using the averaged modal shapes identified through the adaptive method and those reported in [72].

It is worth noting that, in Fig. 10, considering the adaptive procedure, the delay in estimated modal parameters seems to increase when important variations in frequency occur and the filter bank is updated. This is due to the fact that 30-seconds windows at the beginning of each damage scenarios (i.e., the interval between the black and green vertical dashed lines) are processed through the filter bank of the previous scenario while a new window of data is recorded to perform the updating procedure. The parameters identified in these intervals are generally characterized by higher error with respect to the values identified after filter updating. However, the identification latency is the same as the two-step implementation. Considering also filter updates, which nevertheless take place only at the occurrence of specific conditions, the maximum latency in the estimation of modal parameters through the updated filters would be 43.27 seconds in this application. By comparing the frequency values of Fig. 10, it can be noted that, except for the fourth mode in conditions U and A, the parameters estimated by the adaptive procedure approximate the reference ones even under substantial variations, with latency due to filter updating. It is also possible to observe how estimated instantaneous natural frequencies correspond to the ridges of the spectrogram obtained by means of the STFT, also reported in Fig. 10.

Both instantaneous frequencies obtained through the two proposed variants have been processed through a median filter with the same window of 300 samples in order to make instantaneous trends more readable since DESA-1 produces results that are very sensitive to noise. However, in Fig. 10, it can be observed that the adaptive method generally produces smoother trends. In fact, by applying the adaptive procedure, even if structural characteristics vary over time, each filter is always centered on the maximum frequency peak of the identified mode and, through the recursive clustering, the noise is minimized by eliminating the frequency components associated with different ODSs. Conversely, if natural frequencies vary and the filters are static, the noise components gradually gain in importance, making identification results noisier. By observing the MAC coefficients of Fig. 12 and 15, considerable improvement can be noticed especially for damage scenario D. In particular, the first three modes are characterized by MAC values higher than 0.93 for every damage scenario, except D, which has a value of 0.85 for the third mode. The fourth mode has undergone an average increment in the accuracy of 0.21, mainly due to the MAC values related to scenarios C and E.

As explained in Section. 3.4, a simplified clustering method that does not involve the calculation of the whole set of operating deflection shapes can also be performed, especially when the length of filters and the decomposition level are high, involving a high computational effort. In a further analysis, considering the fk22 function (see Fig. 1 for the frequency domain representation of the filter bank) and a decomposition level 7, the ratios between the wavelet components have been directly considered as clustering variables. In particular, two different cases have been analyzed: the first involves sensor positions 4 and 6 as masters, while the second is referred to positions 4 and 15. In Fig. 16 the results of the clustering procedure for the two mentioned cases have been reported. With the small circles, the signal components associated with each filter have been represented in the frequency-signal ratio plane. The filled circles refer to case 1, while the empty circles refer to case 2; the gray circles represent low-energy components, while the black ones represent high-energy components. The high-energy components have been organized in clusters,

represented by larger circles, with a radius proportional to the energy component of each cluster and solid borders for case 1 and dashed for case 2.

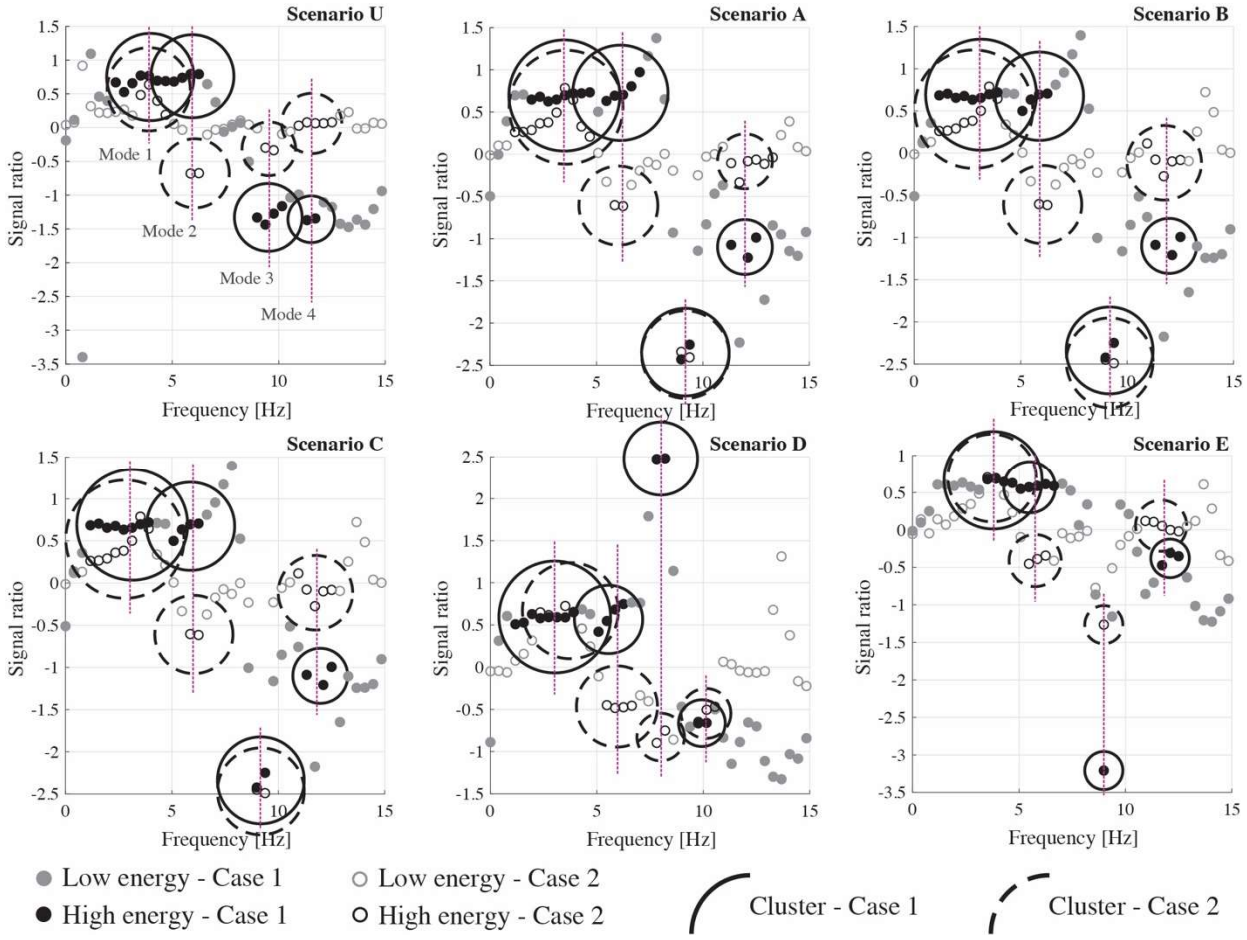

Fig. 16: Simplified clustering procedure.

By observing the diagrams of Fig. 16, as concerns the first case (master sensors 4 and 6), it can be noted that the first two modes are difficult to identify as different clusters, as the ratios between components are very similar, especially for the undamaged condition. On the other hand, as regards the second case (master sensors 4 and 15), the first modes are clearly recognizable, as sensor 15 is arranged on the opposite side with respect to sensor 4 and allows the identification of torsional modes. However, for the third and fourth modes, the signal ratios are poorly accurate in this case, since sensor 15 is close to the nodes of modal shapes. It has to be noted that the clustering procedure can be correctly performed by simultaneously observing both the considered cases. However, by using the MAC-based method the risk of incurring errors that could affect the evaluation of modal parameters is minimized.

4.4 Damage identification

As an example of using the identified modal parameters, a damage identification procedure is applied through the evaluation of the uniform load surface (ULS) [81]. From the knowledge of p

natural frequencies and mass-normalized modal vectors, it is possible to estimate an approximation of the structural flexibility matrix as:

$$\mathbf{F} \cong \sum_{j=1}^{p} \frac{1}{\omega_j^2} \bar{\boldsymbol{\Phi}}_j \, \bar{\boldsymbol{\Phi}}_j^{\mathrm{T}} \tag{16}$$

where $\bar{\boldsymbol{\Phi}}_j$ is the j-th mass-normalized modal vector. Assuming that a unit load vector $\mathbf{p} = [1,1,\ldots,1]^{\mathrm{T}}$ is applied to the analyzed structure, it is possible to estimate the corresponding displacement vector as:

$$\mathbf{u} = \mathbf{F}\,\mathbf{p} \tag{17}$$

Generally, the vector $\mathbf{u}$ is known as the uniform load surface, which in the case of one-dimensional structures degenerates into a line.

In this phase, the natural frequencies of the first three modes, identified through the MAC-based adaptive algorithm, and the related modal shapes have been considered. Only the sensor positions from 1 to 14 (representing the behavior of the west side of the bridge) have been taken into account in the following analyses. Since the mass matrix of the structure is unknown, the modal matrix cannot be mass-normalized. However, if masses are equally distributed along the structure, the mass matrix could be assumed as diagonal, such that $\mathbf{M} = \mu\mathbf{I}$, where μ is a constant value, equal to the mass associated with each DOF of the structure, and $\mathbf{I}$ is the identity matrix. In this way, a matrix proportional to $\mathbf{F}$ can be evaluated. In this application, the mass matrix has been assumed as the identity matrix, since masses are not significantly variable along the longitudinal axis of the bridge.

In Fig. 17(a), the instantaneous uniform load line (ULL) is represented over time, while in Fig. 17(b) the averaged lines for each damage scenario are reported. Since the used flexibility matrix is not mass-normalized, the displacements are not representative of real physical quantities.

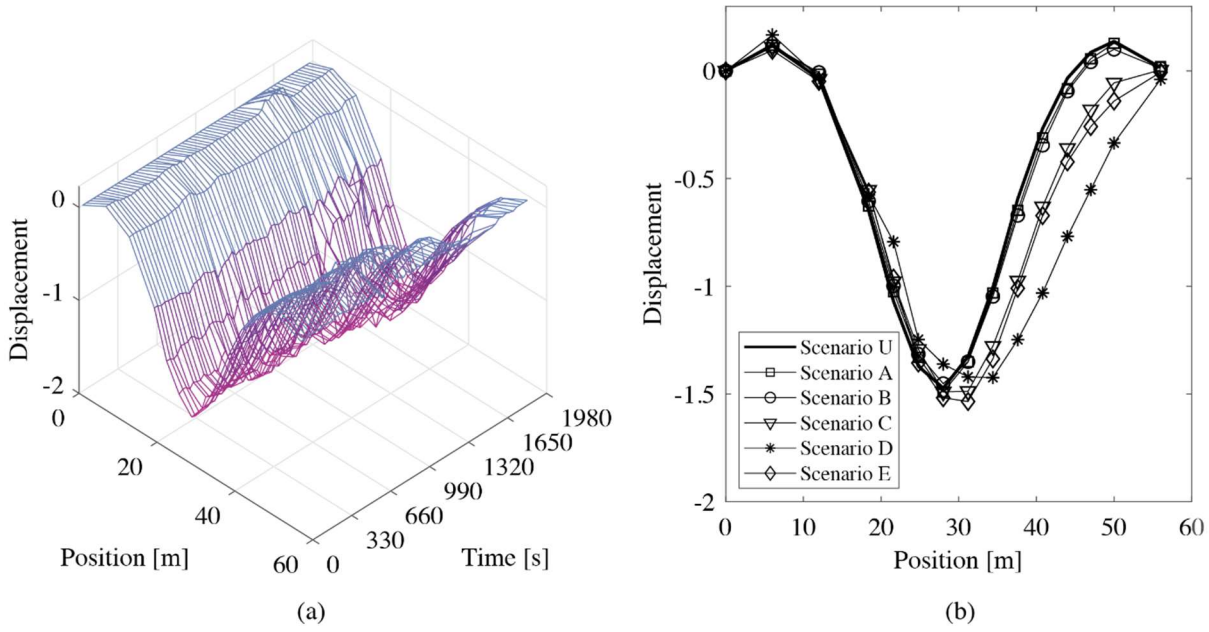

Fig. 17: Mesh interpolation of the instantaneous uniform load lines (a) and averaged lines over time for each damage scenario (b).

In order to perform the damage identification, the absolute variation in terms of displacements (Δ) with respect to the values of the undamaged condition has been considered as a damage-sensitive feature. Both the detection and the localization have been investigated: for the first purpose, the presence of damage is recognized if outliers are identified in the set of computed variations, while the second purpose is accomplished by seeking the outlier position. In Fig. 18(a) the real-time damage identification is represented: the instantaneous Δ values computed by using the ULL estimated during the first initialization procedure and the instantaneous ULLs reported in Fig. 17(a) are represented. In Fig. 18(b) the percentage variations computed by using the ULLs of Fig. 17(b) are plotted versus sensor positions (the origin of position axis has been considered on the south border). For both the instantaneous and averaged analyses, the outliers have been evaluated as terms higher than two standard deviations from the mean. In the first case, the outliers have been computed for each time instant, with the instantaneous mean calculated over the sensor positions, while in the second case the analysis has been performed on the static values represented in Fig. 18(b), for each damage scenario.

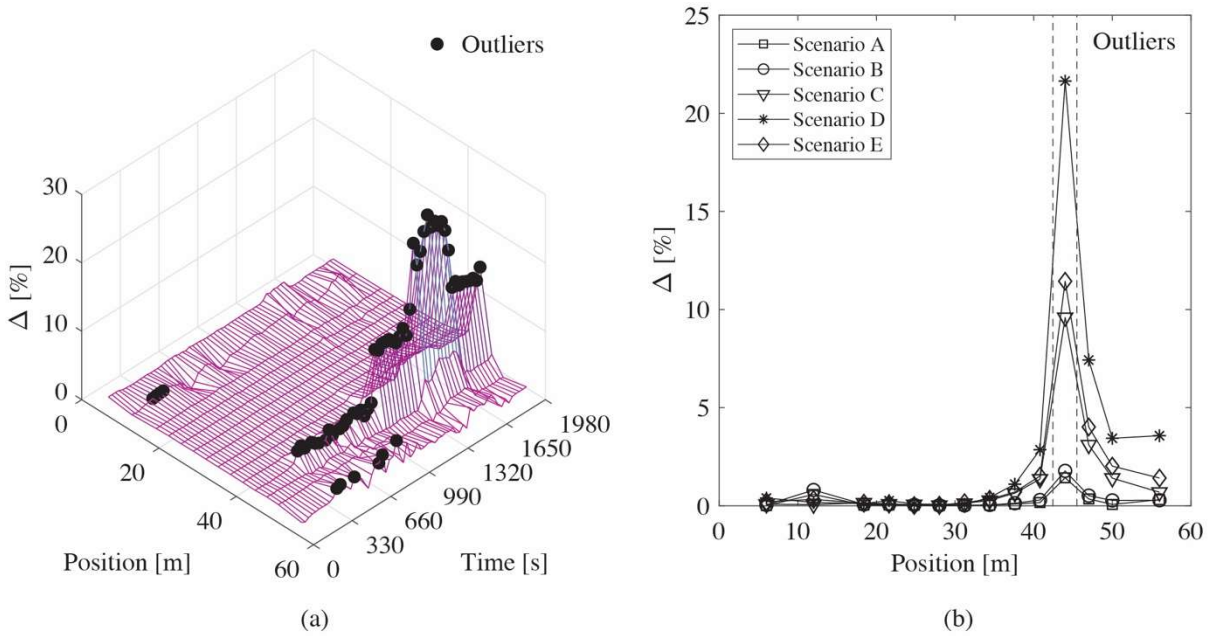

Fig. 18: Instantaneous damage identification (a) and averaged results (b).

It is observable that, for the instantaneous analysis, even by using few modes (i.e., the first three modes in this application), the damage identification has been successfully achieved for each damage scenario from A to E, since a persistent outlier in damage features occurs at the sensor position 11 (i.e., at the damaged pier location). On the other hand, the static evaluation leads to some uncertainty for scenarios A and B, where the maximum value of the damage index is at the sensor position 1 but is also comparable with the variation registered at the position 2. The analysis of instantaneous variation allows therefore the evaluation of the persistence of the identified state of damage. Considering also this aspect, the results of damage identification become more robust to short-term variations due to operational conditions or estimation uncertainties.

5. CONCLUSIONS

In this work, the clustered filter bank decomposition has been proposed as a novel decentralized algorithm for near-real-time identification of instantaneous modal parameters. In particular, the CBF decomposition consists of two main phases: initialization, in which a CFB is built on the basis of a window of collected data, and real-time analysis, in which the sensor nodes process the recorded signals and the monitoring station performs the instantaneous modal identification and post-processing operations. An adaptive variant of the procedure has also been proposed, which consists of the recursive updating of CFB, in order to minimize errors and also efficiently register important variations in modal parameters. It has been shown that the Fejér-Korovkin function is particularly suitable for implementation in this algorithm since it allows the construction of accurate filter banks of modest length.

The identification procedure performed by using TEO has been shown to be particularly fast and sufficiently accurate after the application of a median filter, which however involves an increase of the delay. In particular, by performing the two-step procedure, the natural frequencies and modal shapes have been accurately estimated within a percentage variation in terms of frequencies of about 10% with respect to the initial condition. Performing the adaptive procedure instead, the accuracy of estimated modal parameters has been increased for the whole set of damage conditions, with better results for the lower modes.

A simplified variant for the clustering procedure has also been applied by considering only a subset of recordings for the filter bank construction. The results have shown that the efficacy of this method strongly depends on the choice of master sensor positions. However, good results with less computational burden can be obtained by selecting the master sensors not too close to the nodes of the main modal shapes.

In order to test the quality of estimated parameters, an example of near-real-time damage identification has been performed by using the uniform load surface method. For this purpose, the instantaneous uniform load lines have been computed over time and the percentage variation in terms of displacements has been considered as a damage-sensitive feature. Then, outlier analyses have been performed in order to detect and locate the damage. Both with the instantaneous estimates and the averaged results, damage localization has been successfully fulfilled.

The proposed algorithm has thus demonstrated that it can provide good estimates of time-varying modal parameters under non-stationary excitation together with operational speed and low computational burden. The characteristics of the algorithm make it particularly suitable for emerging WSSN-based monitoring systems. Moreover, different parameters for the construction of the most suitable CFB can be selected based on the specific application, controlling the latency of identified parameters, the noise sensitivity, and the decomposition efficiency for closely-spaced modes.

ACKNOWLEDGEMENTS

The authors would like to thank the Vienna Consulting Engineers (VCE) company for providing the data recorded during the experimental campaign carried out on the S101 Bridge. This research did not receive any specific grant from funding agencies in the public, commercial, or not-for-profit sectors.

APPENDIX A: COMPUTATIONAL COMPLEXITY

A.1 Computational complexity of Step 1

Initialization is a centralized procedure consisting of the processes described in Section 3.2. Since in this phase SWPT is performed through convolutions between a-priori known sequences, the considered complexity is that of the fast convolution algorithm, which allows the computation of each convolution as:

$$y_k[\tau] = \mathrm{IDFT}_M\{\mathrm{DFT}_M\{x[\tau]\} \cdot \mathrm{DFT}_M\{d_k[\tau]\}\} \tag{A.1}$$

where $\mathrm{DFT}_M\{\,\}$ and $\mathrm{IDFT}_M\{\,\}$ denote the Discrete Fourier Transform of length M and its inverse, respectively. In relation (A.1), in order to allow simple multiplications between the terms of DFTs, they have to be of the same length. To this aim, it is possible to extend $x[\tau]$ and $d_k[\tau]$ through zero-padding, in order to have a common length of $M = s + \bar{N} - 1$. Since the length of the analyzed signal is user-defined, it is also possible to choose s such that $s \geq \bar{N}$ and $M = 2^q$, with $q \in \mathbb{Z}^+$. In this case, the DFTs in (A.1) can be computed through radix-2 FFT and the computational complexity of the SWPT can be expressed as reported in Tab. A.1, together with the complexity and storage space required by each process of Step 1. Here, the storage space is intended as the number of elements stored in memory for each process. Moreover, the values in $()_{add}$, $()_{mul}$, $()_{div}$, $()_{com}$, and $()_{sqrt}$ denote the number of additions/subtractions, multiplications, divisions, comparisons, and root square operations, respectively, r is the number of sensors, while c is the number of clusters identified before the energy-based selection.

In order to reduce the computational burden of Step 1, it is possible to limit the analysis to a selected frequency range, computing only a subset of the 2^n wavelet components, and therefore generating a CFB able to identify the vibration modes whose frequencies are contained in the considered range. Therefore, in Tab. A.1, $W \leq 2^n$ denotes the number of wavelet components considered in the initialization step.

Tab. A.1: Computational complexity of each process of Step 1

Process	Complexity	Storage space
SWPT	$3Wr\left[(M\log_2 M)_{add} + \left(\frac{M}{2}\log_2 M - \frac{M}{6}\right)_{mul}\right]$	$W[\bar{N} + rM]$
ODS	$W(r-1)[(s-1)_{add} + (s)_{mul} + (1)_{div}]$	Wr
MAC	$(W-1)[3(r-1)_{add} + (3r+2)_{mul} + (1)_{div}]$	$W-1$
Clustering	$(W-1)_{com}$	-
RMS energy	$Wr\left[(s+r-1)_{add} + (s)_{mul} + (1)_{div} + (1)_{sqrt}\right] - (c)_{add}$	Wr
Energy-based	$(c)_{com}$	-

selection		

In this evaluation, only the strictly necessary operations have been counted. In fact, the coefficients of a complete MAC matrix would be W^2 but, in this case, since only consecutive components can be grouped in the same cluster, the MAC coefficients necessary to verify the condition (6) of Section 3.2 are $W-1$, corresponding to the elements next to the main diagonal of the complete MAC matrix (i.e., $MAC_{k,k+1}$, with $k = 1, \dots, W-1$). At the end of Step 1, the CFB has to be built by summing the bandpass filters associated to the decomposition filters contained in each cluster, as described in Section 3.1. Therefore, if the b_k bandpass filters are already stored in the device memory (using WN storage space), up to $(WN-N)_{add}$ additional operations are necessary to obtain the CFB.

A.2 Computational complexity of Step 2

Following the centralized initialization step, the monitoring system enters a decentralized processing phase. This section describes the computational complexity of the activities performed to obtain each instantaneous parameter, calculated as new data is recorded.

Assuming N the length of the generic filter b_{k_1,k_m} in the relation (3) of Section 3.1, the computational complexity of convolution for p identified modes is given by:

$$\mathcal{C}_c = [(N)_{mul} + (N-1)_{add}]\, p \tag{A.2}$$

per input sample. This procedure needs $N(p+1)+p$ elements stored in memory (i.e., pN elements for the filter bank, N elements for the sliding window of collected data, and p output values). Since convolution is aimed at bandpass filtering, the rate at which it is performed can be reduced according to the frequency band of each filter [49], providing a smaller quantity of new samples for low-frequency components. In this way, the number of operations per second is reduced, making the procedure more efficient and reducing also the number of output values, that can be transferred to the monitoring station with a transfer rate which may even be lower than that of the simple transmission of the unfiltered signal.

Each new value obtained through convolution is then sent to the monitoring station, temporarily stored, and used to compute the instantaneous natural frequencies and modal shapes. In Tab. A.2, the computational complexity of DESA-1 is analyzed, indicating the number of mathematical operations needed to obtain each element of relations (9-10) of Section 3.3 for a given identified mode, computed by using the data collected at a given sensor position. Here, the value in $(\,)_{acos}$ denotes the number of arccosines calculated. Since some values are used to compute the instantaneous frequency at different consecutive instants, the reported number of mathematical operations considers only the elements evaluated for each new sample of data, assuming that the previous values are stored rather than calculated each time. Also, the number of elements stored in memory is shown in Tab. A.2.

Tab. A.2: Computational complexity and storage space for the estimation of instantaneous frequency

Element	Usable from previous computations	Computed for each new sample	Storage space	Complexity
y	$y[\tau-2], y[\tau-1], y[\tau], y[\tau+1]$	$y[\tau+2]$	5	-
z	$z[\tau-1], z[\tau], z[\tau+1]$	$z[\tau+2]$	4	$(1)_{add}$
Ψ	$\Psi[z[\tau]]$	$\Psi[y[\tau]], \Psi[z[\tau+1]]$	3	$(1)_{add} + (2)_{mul}$
Ω	-	$\Omega[\tau]$	1	$(2)_{add} + (1)_{mul} + (1)_{div} + (1)_{acos}$

The computational complexity of the instantaneous frequency calculation does not depend on the filter length, but only depends on the number of identified modes p. It can be expressed as:

$$\mathcal{C}_f = [(5)_{add} + (5)_{mul} + (1)_{div} + (1)_{acos}]\, p \tag{A.3}$$

per input sample. The computational complexity of instantaneous shapes depends instead on the number of identified modes and on the number of sensors r:

$$\mathcal{C}_s = [(r-1)_{div}]\, p \tag{A.4}$$

In this last computation, no additional memory is needed, except for the $(r-1)p$ output elements, since the latest values obtained through convolution are directly used, as shown in equation (12) of Section 3.3. Considering also median filtering for de-noising purposes, the complexity increases of:

$$\mathcal{C}_m = [(\mu-1)_{com}]\, p \tag{A.5}$$

per input sample, for each quantity to which the filter is applied. It is observable that, in the decentralized configuration, a consistent part of the computational burden ($\alpha\mathcal{C}_c$ per second) is carried out onboard each node, while $\alpha(\mathcal{C}_f + \mathcal{C}_s + 2\mathcal{C}_m)$ per second lies with the monitoring station, considering the median filter applied to both natural frequencies and modal shapes, where α is a coefficient that takes into account any downsampling ($\alpha \leq \bar{F}_s$, with $\bar{F}_s$ the sampling frequency of the original signal). Considering p and r modest with respect to N and μ, the computational complexity of the instantaneous filtering process can be expressed in the order of $O(N)$ per input sample, while that related to the activities of the monitoring station is not dependent on N, and therefore assumable in the order of $O(\mu)$. On the other hand, using the proposed algorithm in a centralized topology would imply a computational burden of $\alpha(r\mathcal{C}_c + \mathcal{C}_f + \mathcal{C}_s + 2\mathcal{C}_m)$ per second on the monitoring station, which can be expressed in the order of $O(N)$ per input sample, assuming that N is proportional to μ.

APPENDIX B: EVALUATION OF DELAY

Both due to the convolution and the application of DESA-1, a delay is introduced in the estimated modal parameters. In addition, by applying further post-processing operations to restrain the

fluctuations of modal parameters, the delay increases further. In particular, for the proposed algorithm, the total delay δ is given by the sum of three contributions:

$$\delta = \delta_c + \delta_d + \delta_m \tag{B.1}$$

where δ_c is due to the convolution procedure ($\delta_c = (N-1)/2$) [56], δ_d is associated with the DESA-1 ($\delta_d = 2$), and δ_m is related to the smoothing technique: in case of median filtering, $\delta_m = \mu/2$, with the notations used in equation (11) of Section 3.3.

Since the filter bank related to the SWPT is generated through convolutions between dyadic upsampled filters [45], the length of the obtained analysis and synthesis filters increases with the order of the wavelet function and with the level of decomposition. In particular, considering a wavelet with filters length λ, the length of the filters contained in the decomposition (or reconstruction) filter bank related to the n-th level is:

$$\bar{N} = \lambda\,(2^n - 1) - n + 1 \tag{B.2}$$

The length of the final filters used for online signal analysis is thus $N = 2\bar{N} - 1$, because of relation (1) of Section 3.1. In Tab. B.1, the length of the decomposition and reconstruction filters associated with the wavelets already analyzed in Fig. 1 of Section 2 are reported for different levels.

Tab. B.1: Length of the decomposition and reconstruction filters related to the wavelets fk14, db14, sym14, db7, fk22, and db22, at different decomposition levels

Level	fk14 and db7	db14 and sym14	fk22	db22
4	207	417	327	657
5	430	864	678	1360
6	877	1759	1381	2767
7	1722	3550	2788	5582

In general, filters with high order are suitable for applications in the civil field, where closely-spaced modes and high noise components are present. On the other hand, short filters are preferable for real-time identifications in other engineering fields (e.g., flutter tests [1]).

REFERENCES

[1] A. Klepka, T. Uhl, Identification of modal parameters of non-stationary systems with the use of wavelet based adaptive filtering, Mechanical Systems and Signal Processing 47(1-2) (2014) 21–34. http://doi.org/10.1016/j.ymssp.2013.09.001.

[2] S.A. Jang, H. Jo, S. Cho, K.A. Mechitov, J.A. Rice, S.-H. Sim, H.J. Jung, C.B. Yun, B.F. Spencer Jr., G. Agha, Structural health monitoring of a cable-stayed bridge using smart sensor technology: deployment and evaluation, Smart Structures and Systems 6(5-6) (2010) 439-459. http://doi.org/10.12989/sss.2010.6.5_6.439.

[3] J.A. Rice, K.A. Mechitov, S.-H. Sim, T. Nagayama, S.A. Jang, R. Kim, B.F. Spencer Jr., G. Agha, Y. Fujino, Flexible smart sensor framework for autonomous structural health monitoring, Smart Structures and Systems 6(5-6) (2010) 423-438. http://doi.org/10.12989/sss.2010.6.5_6.423.

[4] B. Bhowmik, T., Tripura, B., Hazra, V. Pakrashi, Real time structural modal identification using recursive canonical correlation analysis and application towards online structural damage detection, Journal of Sound and Vibration 468 (2020) 115101. http://doi.org/10.1016/j.jsv.2019.115101.

[5] M.D. Spiridonakos, S.D. Fassois, Parametric identification of a time-varying structure based on vector vibration response measurements, Mechanical Systems and Signal Processing 23 (2009) 2029-2048. https://doi.org/10.1016/j.ymssp.2008.11.004.

[6] J. Li, M. Su, L. Fan, Natural frequency of railway girder bridges under vehicle loads, Journal of Bridge Engineering 8 (2003) 199–203. https://doi.org/10.1061/(ASCE)1084-0702(2003)8:4(199).

[7] V. Pakrashi, A. O' Connor, B. Basu, Effect of tuned mass damper on the interaction of a quarter car model with a damaged bridge, Structure and Infrastructure Engineering 6(4) (2010) 409-421. http://doi.org/10.1080/15732470701816850.

[8] P. Omenzetter, J. Brownjohn, Application of time series analysis for bridge monitoring, Smart Materials and Structures 15 (2006) 129–138. http://doi.org/10.1088/0964-1726/15/1/041.

[9] H.S. Park, B.K. Oh, Real-time structural health monitoring of a supertall building under construction based on visual modal identification strategy, Automation in Construction 85 (2018) 273-289. https://doi.org/10.1016/j.autcon.2017.10.025.

[10] H.S. Park, Y. Shin, S.W. Choi, Y. Kim, An integrative structural health monitoring system for the local/global responses of a large-scale irregular building under construction, Sensors 13 (2013) 9085-9103. http://doi.org/10.3390/s130709085.

[11] Y. Zhan, V. Makis, A. Jardine, Adaptive state detection of gearboxes under varying load conditions based on parametric modelling, Mechanical Systems and Signal Processing 20 (2006) 188–221. https://doi.org/10.1016/j.ymssp.2004.08.004.

[12] M.S. Allen, M.W. Sracic, S. Chauhan, M.H. Hansen, Output-only modal analysis of linear time-periodic systems with application to wind turbine simulation data, Mechanical Systems and Signal Processing 25(4) (2011) 1174–1191. https://doi.org/10.1016/j.ymssp.2010.12.018.

[13] A. Senba, H. Furuya, Implementation algorithms for self-identification of adaptive structures with variable geometric properties, Mechanical Systems and Signal Processing 22 (2008) 1–14. https://doi.org/10.1016/j.ymssp.2007.05.002.

[14] Z. Ni, R. Mu, G. Xun, Z. Wu, Time-varying modal parameters identification of a spacecraft with rotating flexible appendage by recursive algorithm, Acta Astronautica 118 (2016) 49-61. http://dx.doi.org/10.1016/j.actaastro.2015.10.001.

[15] Y. Kaya, E. Safak, Real-time analysis and interpretation of continuous data from structural health monitoring (SHM) systems, Bulletin of Earthquake Engineering 13 (2015) 917-934. https://doi.org/10.1007/s10518-014-9642-9.

[16] A.G. Poulimenos, S.D. Fassois, Parametric time-domain methods for non-stationary random vibration modelling and analysis – a critical survey and comparison, Mechanical Systems and Signal Processing 20 (2006) 763-816. https://doi.org/10.1016/j.ymssp.2005.10.003.

[17] K.A. Petsounis, S.D. Fassois, Non-stationary functional series TARMA vibration modelling and analysis in a planar manipulator, Journal of Sound and Vibration 231 (2000) 1355-1376. https://doi.org/10.1006/jsvi.1999.2738.

[18] F.P. Kopsaftopoulos, S.D. Fassois, A functional model based statistical time series method for vibration based damage detection, localization and magnitude estimation, Mechanical Systems and Signal Processing 39 (2013) 143-161. https://doi.org/10.1016/j.ymssp.2012.08.023.

[19] M.D. Spiridonakos, S.D. Fassois, Adaptable Functional Series TARMA Models for Non-Stationary Signal Modelling, IFAC Proceedings Volumes 45(16) (2012) 1276-1281. https://doi.org/10.3182/20120711-3-BE-2027.00200.

[20] W. Yang, L. Liu, S.-D. Zhou, Z.-S. Ma, Moving Kriging shape function modeling of vector TARMA models for modal identification of linear time-varying structural systems, Journal of Sound and Vibration 354 (2015) 254-277. https://doi.org/10.1016/j.jsv.2015.06.004.

[21] S. Nagarajaiah, B. Basu, Output only modal identification and structural damage detection using time frequency & wavelet techniques, Earthquake Engineering and Engineering Vibration 8(4) (2009) 583-605. http://doi.org/10.1007/s11803-009-9120-6.

[22] T. Kijewski, A. Kareem, Wavelet transforms for system identification in civil engineering, Computer-Aided Civil and Infrastructure Engineering 18 (2003) 339-355. https://doi.org/10.1111/1467-8667.t01-1-00312.

[23] C. Wang, W. Guan, J.Y. Wang, B. Zhong, X. Lai, Y. Chen, L. Xiang, Adaptive operational modal identification for slow linear time-varying structures based on frozen-in coefficient method and limited memory recursive principal component analysis, Mechanical Systems and Signal Processing 100 (2018) 899-925. http://dx.doi.org/10.1016/j.ymssp.2017.06.018.

[24] F. Amini, V. Ghasemi, Adaptive modal identification of structures with equivariant adaptive separation via independence approach, Journal of Sound and Vibration 413 (2018) 66-78. https://doi.org/10.1016/j.jsv.2017.09.033.

[25] R. Ditommaso, M. Mucciarelli, F.C. Ponzo, Analysis of non-stationary structural systems by using a band-variable filter, Bulletin of Earthquake Engineering 10(3) (2012) 895-911. https://doi.org/10.1007/s10518-012-9338-y.

[26] C. Iacovino, R. Ditommaso, F.C. Ponzo, M.P. Limongelli, The Interpolation Evolution Method for damage localization in structures under seismic excitation, Earthquake Engineering and Structural Dynamics 47(10) (2018) 2117-2136. https://doi.org/10.1002/eqe.3062.

[27] R. Ditommaso, G. Auletta, F.C. Ponzo, Damage detection on framed structures: modal curvature evaluation using Stockwell transform under seismic excitation, Earthquake Engineering and Engineering Vibration 14(2) (2015) 265-274. https://doi.org/ 10.1007/s11803-015-0022-5.

[28] Y. Fu, T. Hoang, K. Mechitov, J. Kim, D. Zhang, B.F. Spencer, Sudden event monitoring of civil infrastructure using demand-based wireless smart sensors, Sensors 18(12) 2018 4480. https://doi.org/10.3390/s18124480.

[29] A.B. Noel, A. Abdaoui, T. Elfouly, M.H. Ahmen, A. Badawy, M.S. Shehata, Structural health monitoring using wireless sensor networks: a comprehensive survey, IEEE Communications Surveys & Tutorials 19(3) (2017) 1403–1423. https://doi.org/10.1109/COMST.2017.2691551.

[30] C. Arcadius Tokognon, B. Gao, G.Y. Tian, Y. Yan, Structural health monitoring framework based on Internet of Things: a survey, IEEE Internet of Things Journal 4(3) (2017) 619–635. http://doi.org/10.1109/JIOT.2017.2664072.

[31] J.P. Lynch, K.J. Loh, A summary review of wireless sensors and sensor networks for structural health monitoring, The Shock and Vibration Digest 38(2) (2006) 91–128. http://doi.org/10.1177/0583102406061499.

[32] H. Jo, S.-H. Sim, T. Nagayama, Development and application of high-sensitivity wireless smart sensors for decentralized stochastic modal identification, Journal of Engineering Mechanics 138(6) (2012) 683-694. http://doi.org/10.1061/(ASCE)EM.1943-7889.0000352.

[33] Y. Gao, B.F. Spencer Jr, M. Ruiz-Sandoval, Distributed computing strategy for structural health monitoring, Structural Control and Health Monitoring 13 (2006) 488-507. https://doi.org/10.1002.stc.117.

[34] A.T. Zimmerman, M. Shiraishi, R.A. Swartz, J.P. Lynch, Automated modal parameter estimation by parallel processing within wireless monitoring systems, Journal of infrastructure systems 14(1) (2008) 102-113. https://doi.org/10.1061/(ASCE)1076-0342(2008)14:1(102).

[35] S.-H. Sim, J.F. Carbonell-Márquez, B.F. Spencer Jr, H. Jo, Decentralized random decrement technique for efficient data aggregation and system identification in wireless smart sensor networks, Probabilistic Engineering Mechanics 26 (2011) 81-91. https://doi.org/10.1016/j.probengmech.2010.07.002.

[36] G.J. Yun, S.-G. Lee, J. Carletta, T. Nagayama, Decentralized damage identification using wavelet signal analysis embedded on wireless smart sensors, Engineering Structures 33(7) (2011) 2162-2172. https://doi.org/10.1016/j.engstruct.2011.03.007.

[37] A. Sadhu, S. Narasimhan, A decentralized blind source separation algorithm for ambient modal identification in the presence of narrowband disturbances, Structural Control and Health Monitoring 21 (2014) 282-302. https://doi.org/10.1002/stc.1558.

[38] D. Vakman, On the analytic signal, the Teager-Kaiser energy algorithm and other methods for defining amplitude and frequency, IEEE Transactions on Signal Processing 44(4) (1996) 791-797. https://doi.org/10.1109/78.492532.

[39] Z. Wang, G. Cheng, Recursive Hilbert-Huang transform method for time-varying property identification of linear shear-type buildings under base excitations, Journal of Engineering Mechanics 138(6) (2012). https://doi.org/10.1061/(ASCE)EM.1943-7889.0000357.

[40] C. Bao, H. Hao, Z.-X. Li, Multi-stage identification scheme for detecting damage in structures under ambient excitations, Smart Materials and Structures 22 (2013) 045006. http://dx.doi.org/10.1088/0964-1726/22/4/045006.

[41] M.F. Ghazali, S.B.M. Beck, J.D. Shucksmith, J.B. Boxall, W.J. Staszewski, Comparative study of instantaneous frequency based methods for leak detection in pipeline networks, Mechanical Systems and Signal Processing 29 (2012) 187-200. https://doi.org/10.1016/j.ymssp.2011.10.011.

[42] L.E. Linderman, K.A. Mechitov, B.F. Spencer Jr., TinyOS-based real-time wireless data acquisition framework for structural health monitoring and control, Structural Control and Health Monitoring 20 (2013) 1007-1020. http://doi.org/10.1002/stc.1514.

[43] T.-P. Le, P. Paultre, Modal identification based on continuous wavelet transform and ambient excitation tests, Journal of Sound and Vibration 331(9) (2012) 2023–2037. http://doi.org/10.1016/j.jsv.2012.01.018.

[44] T. Uhl, A. Klepka, Application of wavelet transform to identification of modal parameters of nonstationary systems, Journal of Theoretical and Applied Mechanics 43(2) (2005) 277-296.

[45] G.P. Nason, B.W. Silverman, The stationary wavelet transform and some statistical applications, in: A. Antoniadis, G. Oppenheim (Eds), Wavelets and Statistics, Lecture Notes in Statistics, vol 103, Springer, New York, 1995, pp. 281-299. https://doi.org/10.1007/978-1-4612-2544-7_17.

[46] A.P. Bradley, Shift-invariance in the discrete wavelet transform, in: C. Sun, H. Talbot, S. Ourselin, T. Adriaansen (Eds.), Proceedings of VII Digital Image Computing: Techniques and Applications, Sydney, 2003.

[47] A. Sadhu, Decentralized ambient system identification of structures, Ph.D. Thesis, Civil Engineering, University of Waterloo, Canada, 2013.

[48] D.K. Alves, F.B. Costa, R. Lucio de Araujo Ribeiro, C. Martins de Sousa Neto, T. de Oliveira Alves Rocha, Real-time power measurement using the maximal overlap discrete wavelet-packet transform, IEEE Transactions on Industrial Electronics 64(4) (2017) 3177–3187. http://doi.org/10.1109/TIE.2016.2637304.

[49] M. Vetterli, J. Kovacevic, Wavelets and subband coding, Prentice Hall Ptr., Englewood Cliffs, New Jersey, 1995.

[50] S.G. Mallat, A theory for multiresolution signal decomposition: the wavelet representation, IEEE Transactions on Pattern Analysis and Machine Intelligence 11(7) (1989) 674–693. http://doi.org/10.1109/34.192463.

[51] S. Ravanfar, H. Razak, Z. Ismail, H. Monajemi, An improved method of parameter identification and damage detection in beam structures under flexural vibration using wavelet multi-resolution analysis, Sensors 15(9) (2015) 22750–22775. http://doi.org/10.3390/s150922750.

[52] C.S. Huang, S.L. Hung, C.I. Lin, W.C. Su, A wavelet-based approach to identifying structural modal parameters from seismic response and free vibration data, Computer-Aided Civil and Infrastructure Engineering 20(6) (2005) 408–423. http://doi.org/10.1111/j.1467-8667.2005.00406.x.

[53] W.C. Su, C.S. Huang, C.H. Chen, C.Y. Liu, H.C. Huang, Q.T. Le, Identifying the modal parameters of a structure from ambient vibration data via the stationary wavelet packet, Computer-Aided Civil and Infrastructure Engineering 29(10) (2014) 738–757. http://doi.org/10.1111/mice.12115.

[54] M. Nielsen, On the construction and frequency localization of finite orthogonal quadrature filters, Journal of Approximation Theory 108(1) (2001) 36–52, http://doi.org/10.1006/jath.2000.3514.

[55] M. Varanis, R. Pederiva, The influence of the wavelet filter in the parameters extraction for signal classification: an experimental study, in: Proceeding Series of the Brazilian Society of Applied and Computational Mathematics (CNMAC 2016), 2017. http://doi.org/10.5540/03.2017.005.01.0501.

[56] M. Vetterli, P. Prandoni, Signal processing for communications, EPFL Press, Lausanne, Switzerland, 2008.

[57] R. Brincker, P. Andersen, N. Møller, An indicator for separation of structural and harmonic modes in output-only modal testing, In J.A. Güemes (Ed.), Proceedings of the European COST F3 Conference on System Identification & Structural Health Monitoring, Madrid, Spain, 2000.

[58] J.F. Kaiser, On a simple algorithm to calculate the 'energy' of a signal, in: International Conference on Acoustics, Speech, and Signal Processing (ICASSP-90), Albuquerque, NM, USA, 1990. https://doi.org/10.1109/ICASSP.1990.115702.

[59] E. Kvedalen, Signal processing using the Teager Energy Operator and other nonlinear operators, Candy Scientific Thesis, University of Oslo, Norway, 2003.

[60] P. Maragos, J.F. Kaiser, Energy separation in signal modulations with application to speech analysis, IEEE Transactions on Signal Processing 41 (1993) 3024-3051. https://doi.org/10.1109/78.277799.

[61] A. Ahrabian, D. Looney, L. Stankovic, D.P. Mandic, Synchrosqueezing-based time-frequency analysis of multivariate data, Signal Processing 106 (2015) 331-341. http://dx.doi.org/10.1016/j.sigpro.2014.08.010.

[62] M.S. Cao, G.G. Sha, Y.F. Gao, W. Ostachowicz, Structural damage identification using damping: a compendium of uses and features, Smart Materials and Structures 26 (2017). https://doi.org/10.1088/1361-665X/aa550a.

[63] Y.-H. Wang, C.-H. Yeh, H.-W. Vincent Young, K. Hu, M.-T. Lo, On the computational complexity of the empirical mode decomposition algorithm, Physica A 400 (2014) 159-167. http://dx.doi.org/10.1016/j.physa.2014.01.020.

[64] V. Zarzoso, A.K. Nandi, Adaptive blind source separation for virtually any source probability density function, IEEE Transactions on Signal Processing 48(2) (2000) 477-488. https://doi.org/10.1109/78.823974.

[65] L.D. Avedaño-Valencia, S.D. Fassois, Gaussian Mixture Random Coefficient model based framework for SHM in structures with time–dependent dynamics under uncertainty, Mechanical Systems and Signal Processing 97 (2017) 59-83. http://dx.doi.org/10.1016/j.ymssp.2017.04.016.

[66] L.D. Avedaño-Valencia, E.N. Chatzi, K.Y. Koo, J.M.W. Brownjohn, Gaussian process time-series models for structures under operational variability, Frontiers in Built Environment 3 (2017) 69. https://doi.org/10.3389/fbuil.2017.00069.

[67] M.P. Limongelli, Seismic health monitoring of an instrumented multistory building using the interpolation method, Earthquake Engineering and Structural Dynamics, 43 (2014) 1581-1602. http://doi.org/10.1002/eqe.2411.

[68] A. Cabboi, C. Gentile, A. Saisi, From continuous vibration monitoring to FEM-based damage assessment: application on a stone-masonry tower, Construction and Building Materials 156 (2017) 252–265. http://doi.org/10.1016/j.conbuildmat.2017.08.160.

[69] A. Saisi, C. Gentile, A. Ruccolo, Continuous monitoring of a challenging heritage tower in Monza, Italy, Journal of Civil Structural Health Monitoring 8(1) (2017) 77–90. http://doi.org/10.1007/s13349-017-0260-5.

[70] G. Zonno, R. Aguilar, R. Boroschek, P.B. Lourenço, Analysis of the long and short-term effects of temperature and humidity on the structural properties of adobe buildings using continuous monitoring, Engineering Structures 196 (2019) 109299. https://doi.org/10.1016/j.engstruct.2019.109299.

[71] Z. Chen, X. Zhou, X. Wang, L. Dong, Y. Qian, Deployment of a smart structural health monitoring system for long-span arch bridges: a review and a case study, Sensors 17(9) (2017) 2151. http://doi.org/10.3390/s17092151.

[72] VCE, Vienna Consulting Engineers, Progressive damage test S101 - Flyover reibersdorf, Report nr. 08/2308, 2009.

[73] D.M. Siringoringo, Y. Fujino, T. Nagayama, Dynamic characteristics of an overpass bridge in a full-scale destructive test, Journal of Engineering Mechanics 139(6) (2013). https://doi.org/10.1061/(ASCE)EM.1943-7889.0000280.

[74] M. Dohler, F. Hille, L. Mevel, W. Rucker, Structural health monitoring with statistical methods during progressive damage test of S101 Brigde, Engineering Structures 69 (2014) 183-193. https://doi.org/10.1016/j.engstruct.2014.03.010.

[75] H. Wenzel, D. Pichler, Ambient vibration monitoring, John Wiley & Sons, Ltd, 2005. http://doi.org/10.1002/0470024577.

[76] A. Bârleanu, V. Băitoiu, A. Stan, FIR filtering on ARM Cortex-M3, in: S. Yenduri (ed.), Proceedings of the 6th WSEAS European Computing Conference, Prague, 2012.

[77] A.N. Sloss, D. Symes, C. Wright, ARM system developer's guide: designing and optimizing system software, Elsevier, Morgan Kaufmann Publishers Inc., San Francisco, CA, USA, 2004. https://doi.org/10.1016/B978-1-55860-874-0.X5000-X.

[78] Intel PXA27x Processor Family: Optimization guide, August, 2004.

[79] L. Wang, M.I. Vai, P.U. Mak, C.I. Ieong, Hardware-accelerated implementation of EMD, In: W. Yu, M. Zhang, L. Wang, Y. Song (Eds.), Proceedings of the 3rd International Conference on Biomedical Engineering and Informatics, Yantai, China, 2010. http://doi.org/10.1109/BMEI.2010.5639875.

[80] G. Rilling, P. Flandrin, P. Goncalves, On empirical mode decomposition and its algorithms, In: Proceedings of the IEEE-EURASIP Workshop on Nonlinear Signal and Image Processing NSIP, Volume 3, pp. 8-11, Grado, Italy, 2003.

[81] Z. Zhang, A.E. Aktan, Application of modal flexibility and its derivatives in structural identification, Research in Nondestructive Evaluation 10(1) (1998) 43-61. https://doi.org/10.1007/PL00003899.